FACULTY OF SCIENCE AND TECHNOLOGY

MASTER'S THESIS

Study programme / specialisation: Master of Science in Structural and Mechanical Engineering	The spring semester, 2023 Open
Author: Silje Midtlien Sigurdsen	
Course leader: Sudath C. Siriwardane Supervisor: Sudath C. Siriwardane	
Thesis title: Reuse of offshore steels for buildings: Lateral torsional buckling capacity of corroded beams	
Credits (ECTS): 30	
Keywords: Steel structures, lateral torsional buckling, corrosion, finite element analysis	Pages: 55 + Appendix: 8 Stavanger, 15.06.2023

Abstract

The building industry is responsible for a lot of today's CO_2 emissions. The emissions from the building industry can be reduced by reusing steel from offshore structures. However, there are several challenges related to reusing steel. Offshore structures are subjected to a harsh environment, and corrosion is a significant cause of failure. Corrosion causes material loss, and this will reduce the cross-sectional properties and the bearing capacity. The risk of lateral torsional buckling (LTB) of open cross-sections increases due to material loss. Thus, there need to be more studies on the simulation of the reduced LTB moment capacity of open cross-sections.

The main objective is to study how the remaining LTB moment capacity of I-sections is affected by various corrosion scenarios, and to provide analytical framework for I-sections with varying cross-sections due to corrosion. Analytical LTB moment capacities of the considered beams are compared with those obtained from a linear finite element (FE) analysis. The buckling reduction factor (χ_{LT}) versus non-dimensional slenderness ($\bar{\lambda}_{LT}$) is plotted for eight different beam lengths subjected to various corrosion scenarios. The elastic buckling moment and LTB moment capacity are obtained for each beam in the linear FE analysis, and a plot of the applied moment versus lateral deflection for one beam is provided.

The LTB moment capacities for beams with a constant cross-section obtained from the linear FE analysis is more conservative than the analytical LTB moment capacities. If the length of the corroded section of the beam is reduced, the LTB moment capacity will increase. Some of the shortest beams are subjected to local plate buckling. As a result, the LTB moment capacity of these beams deviates from the results obtained in the analytical approach. For a 15 m long IPE300 beam subjected to 1.41 mm thickness reduction around the entire cross-section, the LTB moment capacity is reduced by 51%. If only 1/3 of the beam length is subjected to the same thickness loss, the LTB moment capacity for the same beam is reduced by 21%.

Acknowledgement

This thesis is enunciated by Sudath C. Siriwardane and marks the end of my Master of Science in Structural and Mechanical Engineering at the University of Stavanger. During the past five years of taking my degree, I have become interested in steel and its properties subjected to various load scenarios and environments. The building industry is responsible for a lot of today's CO_2 emissions. Hence, it is necessary to discover new ways to reduce emissions. In this thesis, I am investigating the LTB capacity of corroded steel for reusing steel from offshore platforms.

Working on this thesis has been challenging, but it has also been quite educational. It has been time-consuming to familiarise relevant theory and ANSYS Workbench. As a result, I have gained more experiences that I can bring with me to future work.

I want to express my deepest gratitude to my supervisor at the University of Stavanger, Sudath C. Siriwardane, for helpful and valuable advice throughout the writing of this thesis. I also wish to thank Ashish Aeran for his knowledge.

Silje M. Sigurdsen
Stavanger, 15.06.2023

Table of contents

List of Tables

List of Figures

Nomenclature

The symbols that are frequently employed in this thesis are described in the following table. All units are SI base units.

Symbol	Definition	Unit
f_y	Yield strength	MPa
f_u	Ultimate strength	MPa
E	Youngs modulus	GPa
G	Shear modulus	MPa
ε	Factor depending on f_y	
h	Height of the cross-section	mm
b	Width of the cross-section	mm
t_w	Web thickness	mm
t_f	Flange thickness	mm
c_w	Width of the web subjected to pressure	mm
c_f	Width of the flange subjected to pressure	mm
I_z	Moment of inertia about the z-axis	mm^4
I_t	Torsion constant	mm^4
I_w	Warping constant	mm^6
W_y	Section modulus	mm^3
L	Beam length	mm
M_{cr}	Elastic critical moment	kNm
α_m	Moment modification factor	
ϕ_{LT}	A function used to define the reduction factor	
α_{LT}	Imperfection factor for lateral torsional buckling	
$\bar{\lambda}_{LT}$	Non-dimensional slenderness ratio for buckling	
χ_{LT}	Reduction factor for buckling	
$M_{b,Rd}$	Lateral torsional buckling moment capacity	kNm
γ_{M1}	Safety factor	
C(t)	Corrosion depth	mm

t	The lifespan of the structure	Years
t_0	The lifespan of corrosion protection	Years
A	Parameter used to define the corrosion depth	mm
B	Parameter used to define the corrosion depth	

1 Introduction

1.1 Background and motivation

The building industry is responsible for almost 40% of global carbon dioxide (CO_2) emissions. According to the Paris Agreement, the building industry is required to reduce its CO_2 emissions [1]. The existing and future buildings should use less energy, and the emissions from the building process must be reduced. One way to reduce building process emissions is by using materials with lower emissions.

Currently, 12 concrete facilities, 62 fixed steel facilities, and 20 floating steel facilities operate on the Norwegian shelf. Some facilities will be closed and decommissioned in the coming years [2]. Decommissioning is dismantling offshore platforms, including removing and emptying the platform, to rinse and restore the seabed. Typically, offshore platforms consist of a topside and a jacket, as illustrated in Figure 1-1. Offshore jackets are often made of steel or concrete. To a considerable extent, the topside is made from high-quality steel to resist harsh offshore weather conditions.

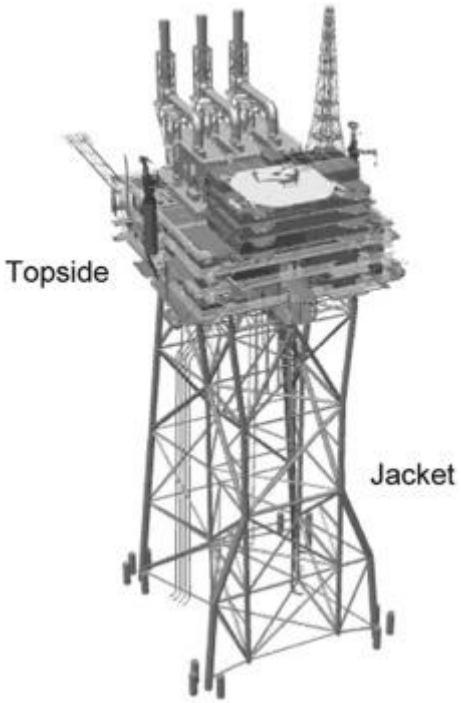

Figure 1-1: General layout of an offshore platform [3]

The most frequent solution for decommissioning an offshore platform is transporting the topside to a scrap yard on shore. All the debris is sorted by source, and the steel will be chopped up and distributed to European steelworks for recycling. Due to the high-quality steel employed in offshore structures, the steel will be melted and reused in new steel products to increase the quality of the new steel [4].

Nordic Circles, a new company in Bergen in Norway, specialises in upcycling steel from decommissioned ships and offshore platforms. Upcycling steel involves reusing the steel without melting it [5]. Nordic Circles claims that upcycling steel, rather than recycling, will reduce CO_2 emissions.

1.2 Problem statement/research gaps

There are various challenges related to reusing steel as load-bearing elements. Reusing steel as load-bearing elements must be done carefully, as the material properties can be reduced due to corrosion, fatigue, or decommissioning. The decommissioning process should be conducted in a way that does not affect the quality of the steel. Because the current offshore structures are not built to be reused, reusing members or more extensive parts of the structure may be challenging. New steel has a material certificate that guarantees the steel properties. A similar guarantee is a necessity to confirm the quality of reused steel. It is also essential that the cost of reused steel should encourage companies to utilise reused steel rather than new steel. In other words, there are several holes to cover regarding this topic.

As a result of extending the lifespan of old structures and building new structures, the amount of exposed steelwork is increasing. Due to environmental exposure, many of these structures are subjected to corrosion, which can reduce the bearing capacity. Corrosion damage is a significant problem for steel structures [6].

1.3 Objectives

It is necessary to have more studies on the simulation of the remaining LTB moment capacity of corroded I-sections. Steel subjected to various damages and degradations can behave significantly differently from undamaged steel. The remaining LTB moment capacity of IPE300-beams from offshore structures subjected to uniform corrosion will be studied in this thesis. An analytical approach is provided based on Eurocode 3 [7]. However, this only

applies to beams where the section is constant for the entire beam. Currently, there needs to be more analytical framework for beams with varying cross-sections. The main objective in this thesis is to study how common corrosion scenarios affect the remaining LTB moment capacity for IPE300-beams. The second objective is to provide an analytical framework for I-beams with varying cross-sections due to uniform corrosion.

1.4 Outline of the thesis

Chapter 2 overviews the current guideline for LTB of uncorroded beams. This method is described in Eurocode 3. This chapter also suggests how to calculate the LTB moment capacity for a beam that is uniformly corroded around the entire section.

Chapter 3 includes the theory about corrosion for offshore structures. This includes types of corrosion, precluding measures, corrosion rate, and the remaining effective cross-sectional properties due to corrosion.

Chapter 4 will focus on a parametric study of beams subjected to uniform corrosion on the entire beam length. Eight beam lengths and two different corrosion cases will be studied. The material and section properties will be presented, along with the elastic critical moment, non-dimensional slenderness ratio, buckling reduction factor, and LTB moment capacity of every beam.

Chapter 5 involves a FE analysis performed in ANSYS Workbench. The beams from Chapter 4 will be investigated, including two additional corrosion cases. The elastic critical moment will be found by providing a linear analysis. The non-dimensional slenderness ratio, buckling reduction factor, and LTB moment capacity of every beam are calculated. Theory for linear and nonlinear analyses will be carried out.

Chapter 6 and 7 provides a comparison and discussion of the results in Chapter 4 and 5, including a conclusion. In the end, there are appendices, which include the utilised MATLAB codes in Chapter 4.

2 Current guidelines for LTB

Lateral torsional buckling is a stability problem that can occur for long, tall beams without lateral restraints. Figure 2-1 shows that the beam will buckle by lateral deflection and twist. The applied moment will function as a component torque and cause rotation about the longitudinal axis. Material loss in the flanges and web will reduce the section properties, such as warping resistance and torsional properties. Consequently, this will reduce the LTB capacity of the beam [8]. This thesis will investigate the remaining LTB moment capacity of corroded steel beams.

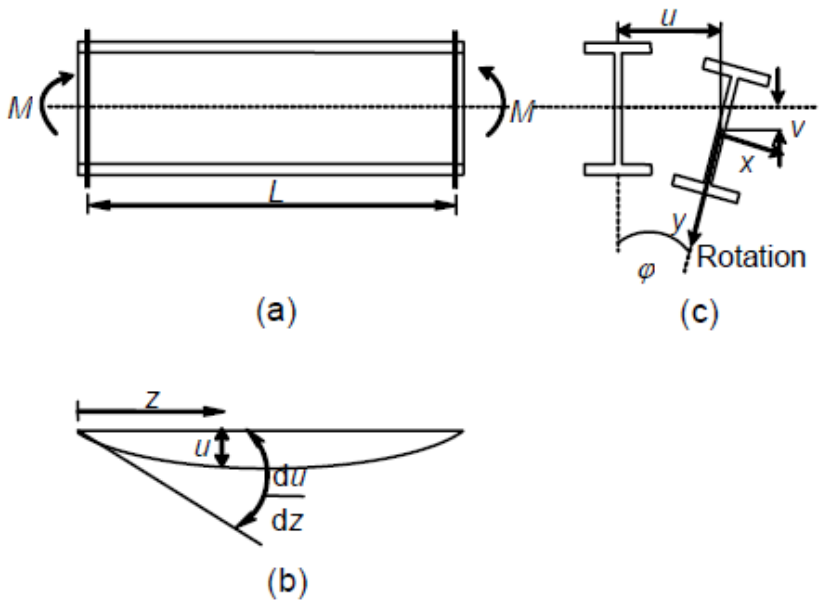

Figure 2-1: Lateral torsional buckling of a simply supported I-section. a) Elevation, b) Plan on the longitudinal axis, c) Section [8]

2.1 Class classification

The class classification is done according to the NS-EN 1993-1-1 5.6 [7] for non-corroded steel. Equation 2.1-1 defines the factor ε for both corroded and non-corroded steel.

$$\varepsilon = \sqrt{235/f_y} \qquad \text{Eq. 2.1-1}$$

For H- and I-sections, the cross-sectional class is determined by the relationship c/t for both web and flange. Figure 2-2 provides a schematic representation of the dimensions of the

cross-section. Equation 2.1-2 and 2.1-3 indicate the depth of the web and flange. The hot-rolled radius is neglected.

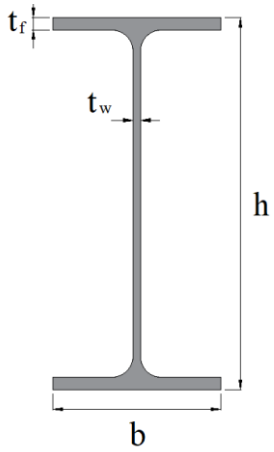

Figure 2-2: Schematic representation of the cross-sectional dimensions

Depth of the web:

$$c_w = \mathrm{h} - 2 \cdot t_f \qquad \text{Eq. 2.1-2}$$

Depth of the flange:

$$c_f = \frac{(b - t_w)}{2} \qquad \text{Eq. 2.1-3}$$

The four classes are defined in NS-EN 1993-1-1 5.5.2 [7]:

- Class 1: Plastic hinges can occur with the rotation capacity necessary for plastic analysis without reducing the design plastic moment capacity of the cross-section.
- Class 2: Design plastic moment capacity can develop, but the cross-section has limited rotational capacity due to local buckling of cross-sectional parts.
- Class 3: The stress in the most exposed point can reach the yield strength due to the elastic distribution of stresses, but the development of design plastic moment capacity is prevented by local buckling.
- Class 4: Local buckling will occur when the yield strength is reached in one or more parts of the cross-section.

The web and flange can be classified separately; then, the cross-section will be classified after the least favourable class of the web and flange.

The relationship c_c/t_c for the web and the flange can be used to determine the cross-sectional class for the corroded section. The class classification of corroded sections can be determined with Equations 2.1-4 and 2.1-5. However, these equations can solely be employed for sections subjected to uniform corrosion around the entire section.

Depth of corroded web:

$$c_{wc} = \mathrm{h}_c - 2 \cdot t_{f,c} \qquad \text{Eq. 2.1-4}$$

Depth of corroded flange:

$$c_{fc} = \frac{(b_c - t_{w,c})}{2} \qquad \text{Eq. 2.1-5}$$

$t_{f,c}$ and $t_{w,c}$ are the corroded flange and web thickness. b_c and h_c are the total width and height of the corroded section. In these equations, the hot-rolled radius is neglected.

2.2 Buckling capacity of uniformly corroded sections

NS-EN 1993-1-1 6.3.1 [7] describes the current method to calculate the LTB moment capacity of steel. In this chapter, the equations from Eurocode 3 are adapted to a proposed framework for a corroded section. Although, these equations are only suitable for beams subjected to uniform corrosion around the entire section. The beam must be of uniform section. The axes on the cross-section are illustrated in Figure 2-3.

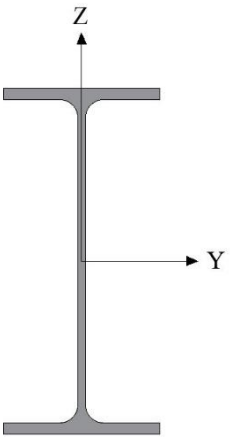

Figure 2-3: Schematic representation of the axes

Moment of inertia about the z-axis for the corroded I-section:

$$I_{z,c} = 2 \cdot \left(\frac{t_{f,c} \cdot {b_c}^3}{12} \right) + \frac{c_{wc} \cdot {t_{w,c}}^3}{12} \qquad \text{Eq. 2.2-1}$$

Torsion constant for the corroded I-section:

$$I_{t,c} = 2 \cdot \left(\frac{b_c \cdot {t_{f,c}}^3}{3} \right) + \frac{c_{wc} \cdot {t_{w,c}}^3}{3} \qquad \text{Eq. 2.2-2}$$

Warping constant for the corroded I-section:

$$I_{w,c} = \frac{{b_c}^3 \cdot (h_c - t_{f,c})^2 \cdot t_{f,c}}{24} \qquad \text{Eq. 2.2-3}$$

The section modulus for a corroded section $W_{y,c}$ depends on the section class:

- Class 1 and 2: $W_{y,c} = W_{pl,y,c}$
- Class 3: $W_{y,c} = W_{el,y,c}$
- Class 4: $W_{y,c} = W_{eff,y,c}$

Plastic section modulus for corroded I-section:

$$W_{pl,y,c} = 2 \cdot \left[b_c \cdot t_{f,c} \cdot \left(\frac{\mathrm{h}_c - t_{f,c}}{2} \right) + \left(\frac{\mathrm{h}_c}{2} - t_{f,c} \right) \cdot t_{w,c} \cdot \frac{\left(\frac{\mathrm{h}_c}{2} - t_{f,c} \right)}{2} \right] \qquad \text{Eq. 2.2-4}$$

A function used to define the reduction factor for the corroded section:

$$\phi_{LT,c} = 0.5 \cdot \left[1 + \alpha_{LT} \cdot (\bar{\lambda}_{LT,c} - 0{,}2) + \bar{\lambda}_{LT,c}{}^2\right] \quad \text{Eq. 2.2-5}$$

The imperfection factor for LTB α_{LT} is determined in Table 2-1:

Table 2-1: Recommended imperfection factor for buckling curves for lateral torsional buckling [7]

Buckling curve	**a**	**b**	**c**	**d**
α_{LT}	0.21	0.34	0.49	0.76

The buckling curves for rolled I-sections are determined in Table 2-2:

Table 2-2: Recommended buckling curve for lateral torsional buckling [7]

Limitation	**Buckling curve**
$h/b \leq 2$	a
$h/b > 2$	b

Non-dimensional slenderness ratio for buckling of the corroded section:

$$\bar{\lambda}_{LT,c} = \sqrt{\frac{f_y \cdot W_{y,c}}{M_{cr,c}}} \quad \text{Eq. 2.2-6}$$

$M_{cr,c}$ is the elastic critical moment.

Buckling reduction factor of a corroded beam with constant section:

$$\chi_{LT,c} = \frac{1}{\phi_{LT,c} + \sqrt{\phi_{LT,c}{}^2 - \bar{\lambda}_{LT,c}{}^2}} \leq 1{,}0 \quad \text{Eq. 2.2-7}$$

The design moment capacity for LTB of corroded section with no lateral stiffeners:

$$M_{b,Rd,c} = \chi_{LT,c} \cdot W_{y,c} \cdot \frac{f_y}{\Upsilon_{M1}} \quad \text{Eq. 2.2-8}$$

f_y is the yield strength, and Υ_{M1} is the safety factor.

3 Corrosion on offshore structures

The topside of an offshore platform is subjected to atmospheric corrosion due to rain, mist, or condensation. Iron corrodes if the relative humidity exceeds 60%. If the relative humidity exceeds 80%, the rust can absorb water and increase the corrosion rate. Atmospheric corrosion will be influenced by the temperature as well. The reaction rate will typically increase due to an increase in temperature. Temperature influences the relative humidity, and temperature changes can cause condensation. Condensation can cause corrosion inside a structure, which can be challenging to locate. Chloride ions will occur at marine locations and tend to increase the corrosion rate. Atmospheric corrosion is not a form of corrosion; it is a collective term for corrosion on surfaces exposed to the air [9].

Ageing offshore structures are subjected to material degradation due to fatigue, and corrosion is a significant cause of failure. With time, the mechanical properties of steel are influenced by changes due to corrosion. Corrosion causes material loss. Hence, this will lead to a reduction of the section properties and the load-bearing capacity. The most common form of corrosion is uniform corrosion. This type of corrosion can reduce structural stiffness and cause local structural collapse. Offshore structures are also subjected to pitting and crevice corrosion, which are forms of localised corrosion and corrosion fatigue. A corrosion protection system (CPS) can be employed to prevent corrosion. Although this system has a typical lifespan of 5-15 years, it has no effect in the splash zone, and localised corrosion can start before the effectiveness of the CPS reduces [10].

3.1 Forms of corrosion

Uniform corrosion occurs at the surface area of a material exposed to a corrosive environment, such as the atmosphere. This will cause a slow thinning of the cross-sectional area. Proper materials or a protective finish can minimise this corrosion type [11].

Crevice and pitting corrosion are often considered together, although they are initiated differently. Crevice corrosion may occur when only a part of a metal is in a restricted or shielded environment, and the rest is exposed to a large electrolyte volume. This form of corrosion occurs slowly over the exposed metal surface. Pitting corrosion can occur at weak metallurgical pints, such as damages, defects, dislocations, inclusions, or precipitates. Environments with high chloride ion content, for example seawater, are the most damaging

environments in conjunction with pitting and crevice corrosion. Stainless steels have poor resistance to crevice corrosion in stagnant seawater.

It is found that the fatigue resistance is reduced in aqueous environments. Corrosion fatigue is a common but dangerous form of corrosion. Cyclic loading in a corrosive environment will result in corrosion fatigue, which can cause a severe reduction of fatigue strength. Cathodic protection on structural steel for offshore platforms forms a suitable environment for developing corrosion fatigue due to lower potentials and hydrogen embrittlement [9].

3.2 Precluding measures for offshore structures

Sufficient design of structures can prevent or reduce the amount of corrosion. It is necessary to ensure that a structure satisfies its function for the designed lifespan by ensuring sufficient safety margins. The structure should be formed so it is easy to inspect, maintain or replace corroded parts. Water and debris traps should be avoided, and sufficient drainage and ventilation should be applied.

Some coatings can be applied to a metal surface to separate the metal from the environment and control the microenvironment on the surface. Coatings for offshore use may be several millimetres thick. There is a considerable amount of diverse paint types, but the primary offshore and marine coating system is a combination of epoxy and urethanes. The epoxy is used for corrosion resistance and adhesion, and urethanes are applied as a topcoat. Epoxy can protect steel and concrete structures in most climates and locations. Jackets on offshore platforms can have coatings up to 5 mm thick by adding quartz particles to increase the thickness. Antifouling paints are applied to the jacket on offshore platforms to prevent organisms from attaching to the immersed areas of the platform. The paint releases toxins into the water, preventing organisms from attaching to the structures. Large growths of barnacles increase the drag force; as a result, the stress levels in the platform increase.

Corrosion can also be avoided by using cathodic and anodic protection. Cathodic protection includes two techniques: The sacrificial anode method and the impressed current method, also known as impressed current cathodic protection (ICCP). For any corrosion cell, the anode will corrode, and the cathode will not corrode. The sacrificial anode method involves applying a material that will be the anode, so the structure becomes the cathode and will be protected

against corrosion. If the current density is too high, the cathode may be damaged. In most cases, this will cause damage to paint coatings, but hydrogen embrittlement may also occur. Zinc, magnesium, and aluminium are suitable materials for anodes and are widely used [9].

The ICCP also involves sacrificial anodes, but the anodes are separated from the structure. The suitable current will be provided from external sources, and the current will be larger than the sacrificial anode method. Therefore, the ICCP is more suitable for larger structures. This method is more effective than the sacrificial anode method but is also more expensive [12].

3.3 Corrosion on topsides

The topside on offshore platforms consists of primary and secondary structures, process equipment, piping, and safety and emergency equipment. There is a considerable range of consequences and associated risks due to the complexity of the topside. Topsides are subjected to atmospheric corrosion. The only cost-effective method for atmospheric corrosion control is coatings. Coatings for topsides should be flexible and UV-resistant. The quality of the coating is influenced by the type of coating, dry film thickness, application method, damages, and maintenance. For topsides, the corrosion often starts in areas with coating damage or where the coating has inadequate quality, like weld seams, edges, and notches. The coating may be damaged by overloads causing stress or reduction of the steel dimensions due to corrosion, dents, repair work, and more. Areas of the structure that is challenging to access can be subjected to undetected corrosion. Water and debris can be trapped on horizontal surfaces and areas without sufficient drainage and cause severe corrosion. Isolation used for fire protection and thermal isolation can hide steel surfaces with corrosion because the isolation material can hold water. The structural integrity of topsides can be subjected to significant consequences due to general or uniform corrosion for an extended period [13].

3.4 Corrosion rate

Uniform corrosion is the most generic corrosion form for topsides, and the effect is time-dependent. Based on various studies, a nonlinear function can simulate the depth of uniform corrosion [10].

$$C(t) = A \cdot (t - t_0)^B \; ; \; t > t_0 \qquad \text{Eq. 3.4-1}$$

Equation 3.4-1 is the nonlinear model for the thickness wastage due to corrosion. This assumes no corrosion when the CPS is effective. t is the structure's lifespan, and t_0 is the CPS's lifespan. A and B are parameters depending on the results from the inspection. These parameters are given in Table 3-1.

Table 3-1: Mean values of the model parameters for uniform corrosion [10]

Inspection findings	**Splash zone area**		**Other areas**	
	A (mm)	**B**	**A (mm)**	**B**
Not performed – unmanned facility or high costs involved	0.3	1	0.1	1
Severe corrosion found – uniform corrosion with many patches and pitting corrosion	0.3	0.823	0.1	0.823
No significant corrosion – slight uniform corrosion with few patches	0.252	0.823	0.084	0.823

The thickness wastage model is quite conservative, and several factors influence the corrosion rate. For example, the corrosion rate for atmospheric corrosion will vary from area to area, depending on the temperature, relative humidity, and local contaminants [9].

3.5 Effective cross-sectional properties due to corrosion wastage

Uniform corrosion will reduce the plate thickness. Consequently, the effective area, second moment of area, torsional constant, and warping constants must be found by considering the plate thickness reduction due to corrosion. This chapter is mainly taken from the article *"Remaining fatigue life estimation of corroded bridge members"* [14]. A schematic representation of the corroded section parameters is given in Figure 3-1.

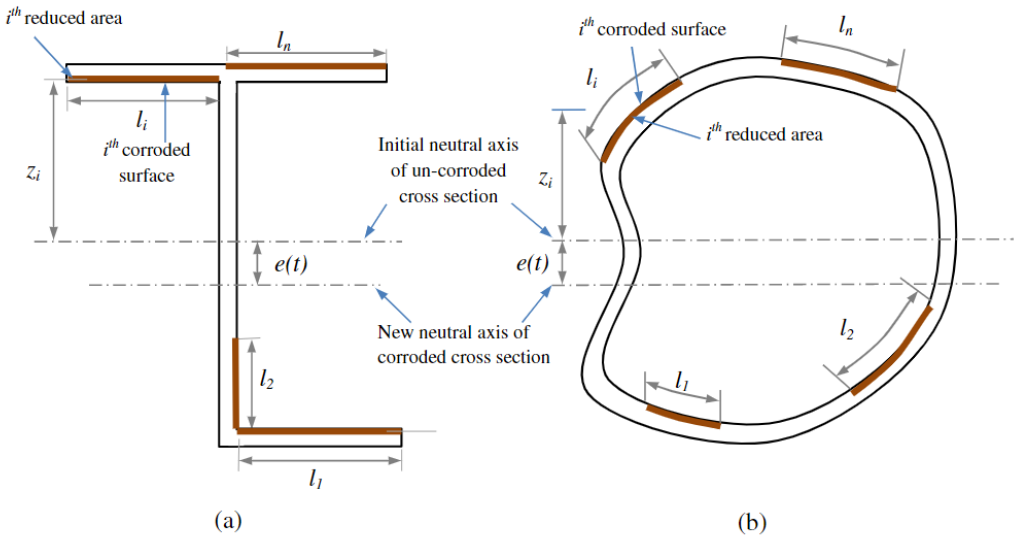

Figure 3-1: Schematic representation of corroded section parameters. (a) Open section and (b) closed section [14]

The formula for the time-dependent effective cross-sectional area is given in Equation 3.5-1. This considers the thickness wastage due to corrosion given in Chapter 3.4.

$$A_c(t) = A_0 - \sum_{i=1}^{n} C_i(t) \cdot l_i \qquad \text{Eq. 3.5-1}$$

A_0 is the initial cross-sectional area, and l_i is the length of corrosion, shown in Figure 3-1. $C_i(t)$ is the thickness wastage due to corrosion at the reduced area of the cross-section.

The calculation of the effective second moment of area about the y-axis of the corroded cross section is given in Equation 3.5-3. This is calculated about the new neutral axis. The distance from the initial neutral axis to the new neutral axis is given in Equation 3.5-2.

$$e(t) = \frac{\sum_{i=1}^{n} C_i(t) \cdot l_i \cdot z_i}{A_c(t)} \qquad \text{Eq. 3.5-2}$$

z_i is the height from the initial neutral axis to the centroid of the reduced area, shown in Figure 3-1.

$$I_{z,c}(t) = I_0 + A_0 \cdot e(t)^2 - \sum_{i=1}^{n} \{\Delta I_i + C_i(t) \cdot l_i \cdot [z_i + e(t)]^2\} \qquad \text{Eq. 3.5-3}$$

I_0 is the initial second moment of area of the cross-section, and ΔI_i is the second moment of the reduced area.

Considering the thickness wastage due to corrosion, the effective torsional constant of the corroded cross-section can be calculated as shown in Equation 3.5-4.

$$I_{t,c}(t) = \frac{1}{3} \cdot \sum_{i=1}^{n} b_i \cdot a_i(t)^2 \qquad \text{Eq. 3.5-4}$$

a_i and b_i are the thickness and length of the reduced area, shown in Figure 3-2.

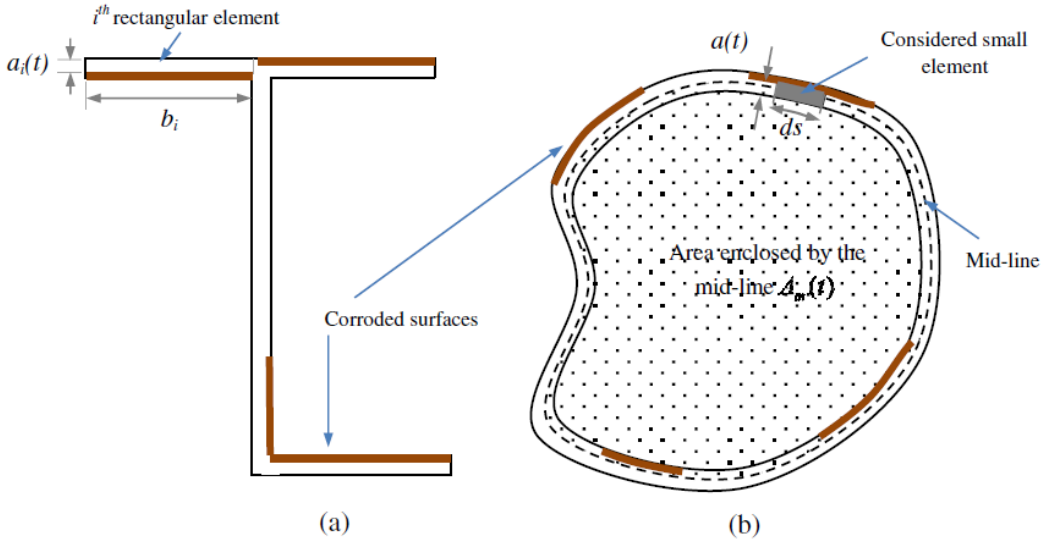

Figure 3-2: Schematic representation of the torsional parameters. (a) Open section and (b) closed section [14]

The effective warping constant of the corroded section is given in Equation 3.5-5 and considers the thickness wastage.

$$I_{w,c}(t) = \int_0^E [\alpha_n(t) - \alpha(t)]^2 \cdot a(t)\, ds \qquad \text{Eq. 3.5-5}$$

Were

$$\alpha(t) = \int_0^S \rho_0(t)\, ds \qquad \text{Eq. 3.5-6}$$

and

$$\alpha_n(t) = \frac{1}{A_c(t)} \cdot \int_0^E \alpha(t) \cdot a(t)\, ds \qquad \text{Eq. 3.5-7}$$

$a(t)$ is the function of time-dependent thickness wastage due to uniform corrosion, $\rho_0(t)$ is the perpendicular distance from the shear centre to the tangent to the centre line of the section wall, shown in Figure 3-3.

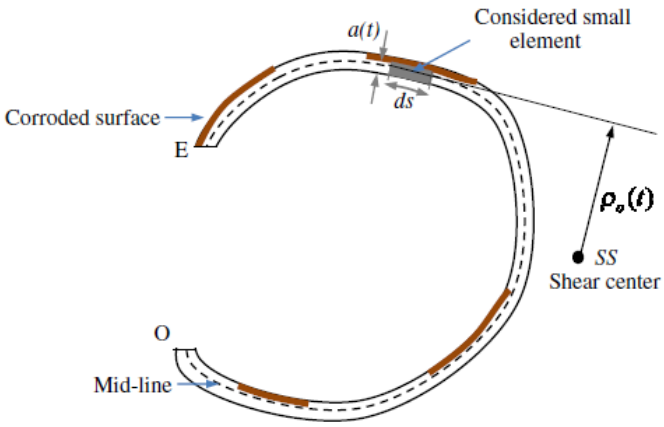

Figure 3-3: Schematic representation of warping parameters of open thin-walled cross-section [14]

3.6 Buckling capacity due to corrosion wastage

Finding the new neutral axis in the z-direction is necessary to calculate the lateral buckling moment capacity. This chapter is mainly taken from the paper *"Lateral torsional buckling capacity of corroded steel beams: A parametric study"* [15]. The distance from the initial neutral axis to the new neutral axis can be found as shown in Equation 3.6-1.

$$e_z(t) = \frac{\sum_{i=1}^{n} C_i(t) \cdot l_i \cdot y_i}{A_c(t)} \qquad \text{Eq. 3.6-1}$$

y_i is the height from the initial neutral axis to the centroid of the reduced area, shown in Figure 3-4.

The effective second moment of area about the z-axis:

$$I_{z,c}(t) = I_{z,0} + A_0 \cdot e_z(t)^2 - \sum_{i=1}^{n} \{\Delta I_{z,i} + C_i(t) \cdot l_i \cdot [y_i + e_z(t)]^2\} \qquad \text{Eq. 3.6-2}$$

$I_{z,0}$ is the initial second moment of area of the cross-section, and $\Delta I_{z,i}$ is the second moment of the reduced area.

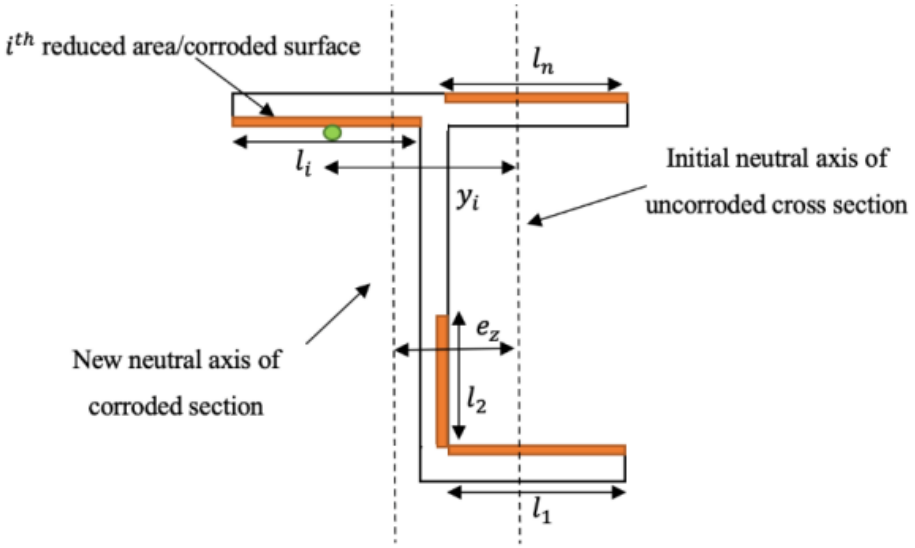

Figure 3-4: Schematic representation of corroded section parameters [15]

The critical elastic moment for a corroded section:

$$M_{cr,c} = \sqrt{\left(\frac{\pi^2 \cdot E \cdot I_{z,c}}{L^2}\right) \cdot \left[G \cdot I_{t,eff} + \left(\frac{\pi^2 \cdot E \cdot I_{w,c}}{L^2}\right)\right]} \qquad \text{Eq. 3.6-3}$$

The plastic modulus for a corroded section can be found as:

$$W_{pl,y,c} = A_{t1}y_{t1} + A_{t2}y_{t2} + A_{c1}y_{c1} + A_{c2}y_{c2} + A_{c3}y_{c3} \qquad \text{Eq. 3.6-4}$$

Were:

Tension part

$A_{t1} = b \cdot t_f$

$A_{t2} = (y_p - t_f) \cdot t_w$

$y_{t1} = y_p - t_f/2$

$y_{t2} = (y_p - t_f)/2$

Compression part

$A_{c1} = b_c \cdot t_{f,c}$

$A_{c2} = (h_w/2) \cdot t_{w,c}$

$A_{c3} = (h_c - y_p - t_{f,c} - h_w/2) \cdot t_w$

$y_{c1} = h_c - y_p - t_{f,c}/2$

$y_{c2} = h_c - y_p - t_{f,c} - h_w/4$

$y_{c3} = (h_c - y_p - t_{f,c} - h_w/2)/2$

A_{t1} and A_{t2} are the areas of the tension part of the section. y_{t1} and y_{t2} are the distances to the plastic neutral axis. A_{c1}, A_{c2}, and A_{c3} are the areas of the compression part of the section. y_{c1},

y_{c2}, and y_{c3} are the distances to the plastic neutral axis. b is the width of the uncorroded part of the section, b_c is the width of the corroded part of the section, h_c is the corroded height, and h_w is the web height.

y_p is the plastic neutral axis and can be found as:

$$T = C$$

$$A_t f_y = A_c f_y$$

$$y_p = \frac{\left[(h_c t_w) - (t_{f,c} t_w) - \left(\frac{h_w}{2} t_w\right) + \left(\frac{h_w}{2} t_{w,c}\right) + (b_c t_{f,c}) - (b t_f) + (t_f t_w)\right]}{2 t_w} \quad \text{Eq. 3.6-5}$$

T and C are the tension and compression force. A_t and A_c are the tension and compression area. The obtained $M_{cr,c}$ and $W_{pl,y,c}$ can be applied to Equation 2.2-6 and 2.2-8 to find the LTB moment capacity $M_{b,Rd,c}$ of a corroded beam.

4 LTB moment capacity: Analytical approach

In this chapter, a parametric study of the LTB moment capacity will be performed. The beam is simply supported and has a uniformly distributed load, illustrated in Figure 4-1. The employed cross-section is IPE300, according to the NS-EN 10 034. The variables in this study are the beam length and corrosion case. Eight different beam lengths will be used: 1.5, 2, 3, 4, 5, 6, 10, and 15 meters, and two different corrosion cases. The objective is to examine the LTB moment capacity of several beams subjected to various cases of uniform corrosion. The applied steel grade is S275JR, where the yield and ultimate strength are $f_y = 275\ MPa$ and $f_u = 430\ MPa$. The safety factor Υ_{M1} is neglected to compare with the FE analysis results in Chapter 5. This method is only applicable to beams with a constant section.

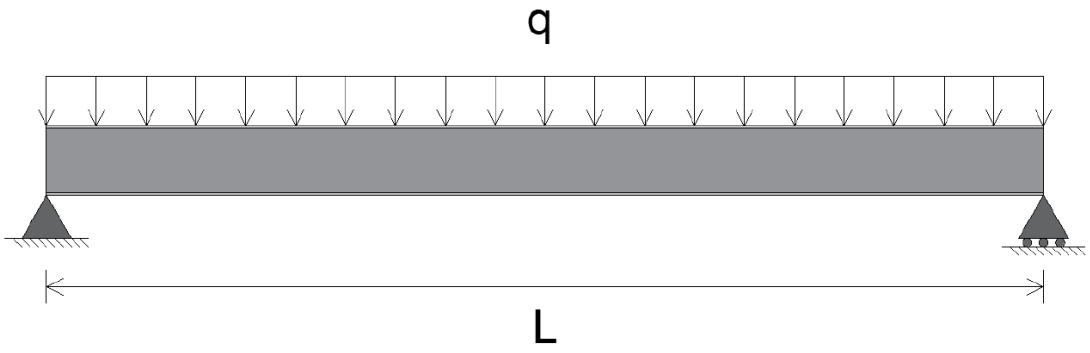

Figure 4-1: The beam with load and supports

4.1 Software

The software utilised for this study is MATLAB R2021a. This programming and numeric computation platform developed by MathWorks can be used to create models, develop algorithms and analyse data. The utilised code for this chapter can be found in Appendix A, B, and C.

4.2 Proposed analytical approach

The LTB capacity of the uncorroded section will be investigated first to compare it with the corroded sections. Two different cases of corrosion will be studied:

- Case 1: Uniform corrosion around the entire section
- Case 2: Uniform corrosion on the bottom flange and bottom half of the web

The material properties are listed in Table 4-1.

Table 4-1: Material properties of the employed steel beam

Material properties	
E (Young's Modulus)	210 GPa
G (Shear Modulus)	81 395 MPa
Poisson's Ratio	0.29
f_y	275 MPa
f_u	430 MPa

The lifespan of oil platforms will vary, and the lifespan will often be extended. As a reference, the Gyda-platform had a lifespan of about 30 years before it was decommissioned [16]. In Chapter 3, the lifespan of the corrosion protection system is assumed to be 5-15 years. Five years will be employed for this study. The A and B parameters in Table 3-1 for *severe corrosion found* and *other areas* will be employed to calculate the corrosion wastage. Only uniform corrosion will be applied; patch and pitting corrosion will be neglected. Consequently, the corrosion wastage is found to be 1.41 mm. The cross-sectional properties are listed in Table 4-2, and the different cross-sections are illustrated in Figure 4-2. IPE300 is a class 1 section. The section subjected to corrosion case 1 is a class 2 section. Thus, the plastic moment capacity can develop for the proposed corrosion scenarios, and $W_{pl,y}$ can be utilised.

Table 4-2: Cross-sectional properties of the employed sections

Cross-sectional properties			
	No corrosion	Case 1	Case 2
Total height	300 mm	297.2 mm	298.6 mm
Web height	278.6 mm	281.4 mm	281.4 mm
Top flange width	150 mm	147.2 mm	150 mm
Bottom flange width	150 mm	147.2 mm	147.2 mm
Top web thickness	7.1 mm	4.3 mm	7.1 mm
Bottom web thickness	7.1 mm	4.3 mm	4.3 mm
Top flange thickness	10.7 mm	7.9 mm	10.7 mm
Bottom flange thickness	10.7 mm	7.9 mm	7.9 mm
$W_{pl,y}$	$6.02 \cdot 10^5\ mm^3$	$4.20 \cdot 10^5\ mm^3$	$4.86 \cdot 10^5\ mm^3$
I_z	$6.03 \cdot 10^6\ mm^4$	$4.18 \cdot 10^6\ mm^4$	$5.11 \cdot 10^6\ mm^4$
I_t	$1.56 \cdot 10^5\ mm^4$	$5.52 \cdot 10^4\ mm^4$	$1.06 \cdot 10^5\ mm^4$
I_w	$1.26 \cdot 10^{11}\ mm^6$	$8.75 \cdot 10^{10}\ mm^6$	$1.03 \cdot 10^{11}\ mm^6$

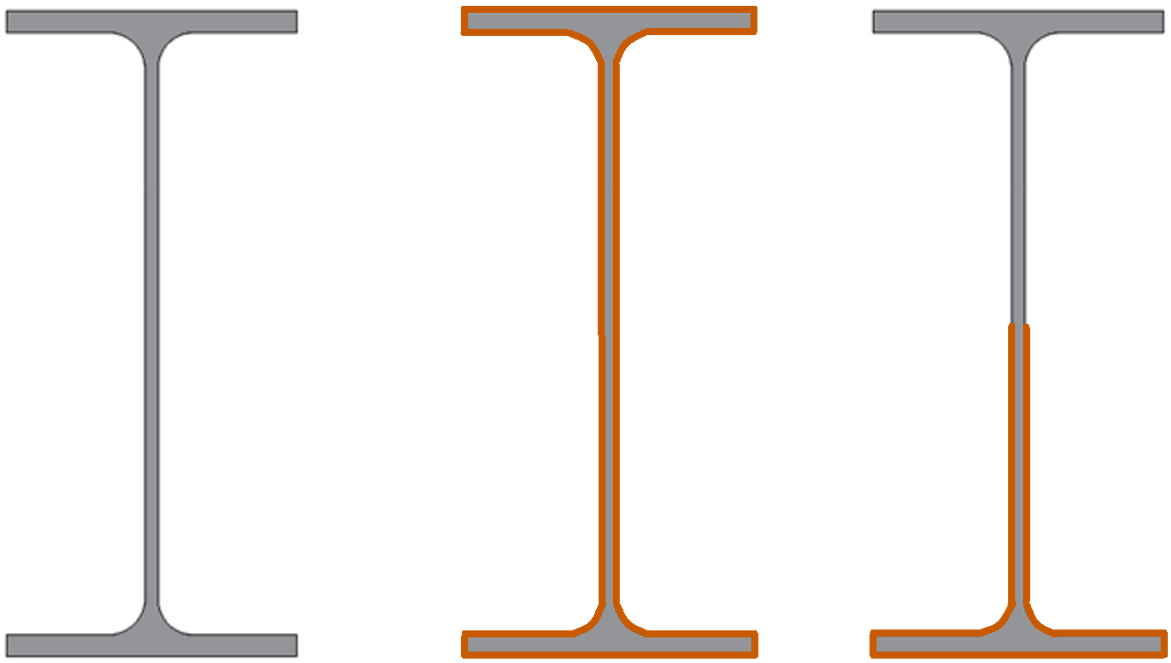

Figure 4-2: Illustration of the provided cross-sections. (a) Uncorroded, (b) uniform corrosion around the entire section, and (c) uniform corrosion on the bottom half of the section.

I_z, I_t, and I_w for corrosion case 2 are found in the *physical properties* in ANSYS DesignModeler. This is provided in Appendix D.

Elastic critical moment [17]:

$$M_{cr} = \alpha_m \cdot M_{zx} \qquad \text{Eq. 4.2-1}$$

were

$$M_{zx} = \sqrt{\left(\frac{\pi^2 \cdot E \cdot I_{z,c}}{L^2}\right) \cdot \left[G \cdot I_{t,c} + \left(\frac{\pi^2 \cdot E \cdot I_{w,c}}{L^2}\right)\right]} \qquad \text{Eq. 4.2-2}$$

E and G are the Youngs and shear modulus. L is the length of the beam, and α_m is the moment modification factor.

4.3 Results

The following tables contain the elastic critical moment (M_{cr}), non-dimensional slenderness ratio ($\bar{\lambda}_{LT}$), buckling reduction factor (χ_{LT}), and LTB moment capacity ($M_{b,Rd}$) for the three cross-sections analysed in this chapter.

Table 4-3: Elastic critical moment, non-dimensional slenderness ratio, buckling reduction factor, and lateral torsional buckling moment capacity for the uncorroded cross-section.

L (m)	$\boldsymbol{M_{cr}}$ **(kNm)**	$\boldsymbol{\bar{\lambda}_{LT}}$	$\boldsymbol{\chi_{LT}}$	$\boldsymbol{M_{b,Rd}}$ **(kNm)**
1.5	955.1	0.42	0.95	157.0
2	557.5	0.55	0.91	150.6
3	271.8	0.78	0.81	133.6
4	170.0	0.99	0.67	111.7
5	121.5	1.17	0.55	91.2
6	94.0	1.33	0.46	75.4
10	49.4	1.83	0.26	43.4
15	31.3	2.30	0.17	28.5

Table 4-4: Elastic critical moment, non-dimensional slenderness ratio, buckling reduction factor, and lateral torsional buckling moment capacity for the cross-section subjected to corrosion case 1.

L (m)	M_{cr} (kNm)	$\bar{\lambda}_{LT}$	χ_{LT}	$M_{b,Rd}$ (kNm)
1.5	647.1	0.42	0.92	105.9
2	371.4	0.56	0.86	99.0
3	174.1	0.81	0.72	82.6
4	104.7	1.05	0.57	65.3
5	72.1	1.27	0.44	51.3
6	54.1	1.46	0.36	41.2
10	26.4	2.09	0.19	22.3
15	16.1	2.67	0.12	14.2

Table 4-5: Elastic critical moment, non-dimensional slenderness ratio, buckling reduction factor, and lateral torsional buckling moment capacity for the cross-section subjected to corrosion case 2.

L (m)	M_{cr} (kNm)	$\bar{\lambda}_{LT}$	χ_{LT}	$M_{b,Rd}$ (kNm)
1.5	788.8	0.41	0.92	123.2
2	457.8	0.54	0.87	115.8
3	220.5	0.78	0.74	98.6
4	136.3	0.99	0.60	80.6
5	96.4	1.18	0.49	65.6
6	74.0	1.34	0.41	54.3
10	38.2	1.87	0.24	31.5
15	24.0	2.36	0.16	20.8

5 LTB moment capacity: FE approach

In this chapter, a FE analysis is performed in ANSYS Workbench to compare with the results in Chapter 4. The beam lengths and corrosion cases will be the same as in the parametric study, and two additional corrosion cases will be investigated.

5.1 Software

ANSYS Workbench 2020 R1 is the utilised software for this study. Workbench is software for FE analyses. A flow chart illustrates the order of the system operation. Figure 5-1 provides the flow chart for the linear Eigenvalue analysis.

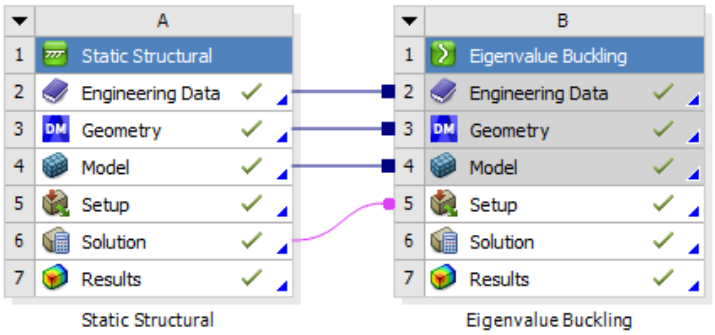

Figure 5-1: Flow chart model of the linear Eigenvalue analysis in ANSYS Workbench

Engineering data is the material model, and provides the material properties. *Geometry* contains a 3D model of the analysed beam. *Model* is where the material properties are assigned to the model and the mesh is generated. *Setup* provides the applied loads and boundary conditions. *Solution* and *results* contain the deformed model and solution information. The engineering data, geometry, model, and solution employed in section A in Figure 5-1 will be shared with section B. Section A will provide a deformed model as a preceding process to the linear Eigenvalue buckling in section B.

The linear Eigenvalue buckling will provide an eigenvalue that can be multiplied by the applied load to determine the elastic critical moment. As this is a linear analysis, the force-displacement curve is idealised. Figure 5-2 illustrates the difference between an idealised response and the actual response of the force-displacement curve. The behaviour is linear elastic, small deformation theory is utilised, and other nonlinear properties are neglected. The linear Eigenvalue buckling requires low computational costs. However, the predicted load is higher than the actual load.

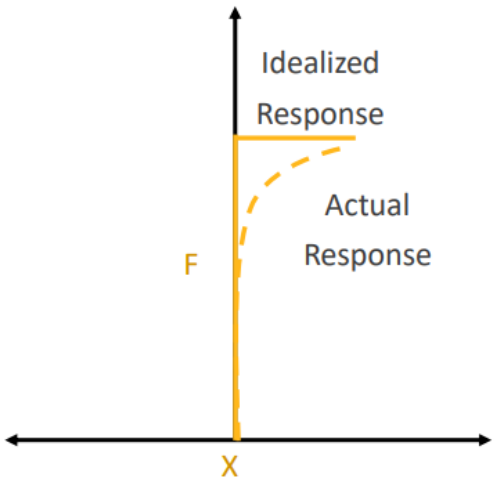

Figure 5-2: Comparison of idealised response versus actual response of the force-displacement curve [18]

Another option to analyse buckling is to perform a nonlinear buckling static analysis. When buckling occurs, the structure is no longer static. As a result, it becomes difficult to solve the problem as a static analysis, and the solutions fail to converge when buckling starts. All the nonlinearities are utilised for this type of analysis, which can be utilised to predict both buckling and local buckling. It is possible to start with a linear buckling analysis to provide an upper limit for the buckling load. By doing so, the estimate will be more accurate. This analysis requires high computational costs. Figure 5-3 provides the flowchart for the nonlinear analysis. The engineering data and solution in section B will be shared with section B and C.

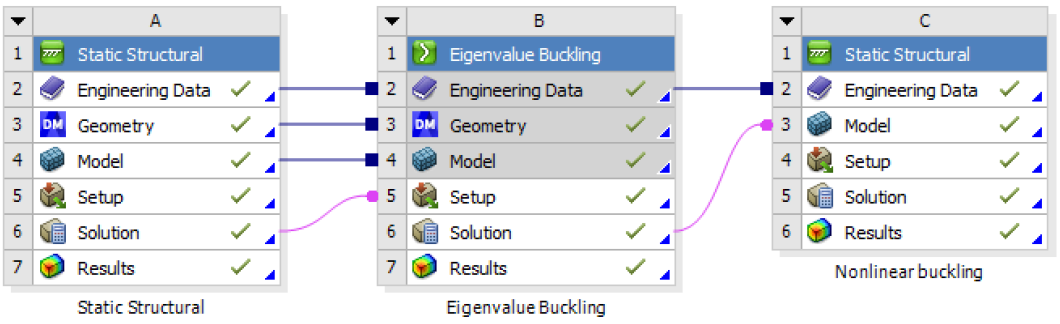

Figure 5-3: Flow chart of the nonlinear buckling static analysis in ANSYS Workbench

5.2 FE simulation

In this study, the beam will be analysed with no corrosion and corrosion case 1 and 2. There will also be two additional corrosion cases:

- Case 3: 1/3 of the length of the beam will be subjected to uniform corrosion around the entire section. Only the middle of the beam length is subjected to corrosion.
- Case 4: 1/3 of the length of the beam will be subjected to uniform corrosion on the bottom flange and bottom half of the web. Only the middle of the beam length is subjected to corrosion.

The cross-sectional properties of corrosion case 3 and 4 are listed in Table 5-1.

Table 5-1: Cross-sectional properties of the employed sections

Cross-sectional properties		
	Case 3	Case 4
Uncorroded sections		
Total height	300 mm	300 mm
Web height	278.6 mm	278 mm
Total width	150 mm	150 mm
Web thickness	7.1 mm	7.1 mm
Flange thickness	10.7 mm	10.7 mm
Hot-rolled radius	15 mm	15 mm
Corroded middle section		
Total height	297.2 mm	298.6 mm
Web height	281.4 mm	281.4 mm
Top flange width	147.2 mm	150 mm
Bottom flange width	147.2 mm	147.2 mm
Top web thickness	4.3 mm	7.1 mm
Bottom web thickness	4.3 mm	4.3 mm
Top flange thickness	7.9 mm	10.7 mm
Bottom flange thickness	7.9 mm	7.9 mm
Top hot-rolled radius	13.6 mm	15 mm
Bottom hot-rolled radius	13.6 mm	13.6 mm

The material properties are the same as in Chapter 4 and can be found in Table 4-1. The five provided types of beams are shown in Figure 5-4.

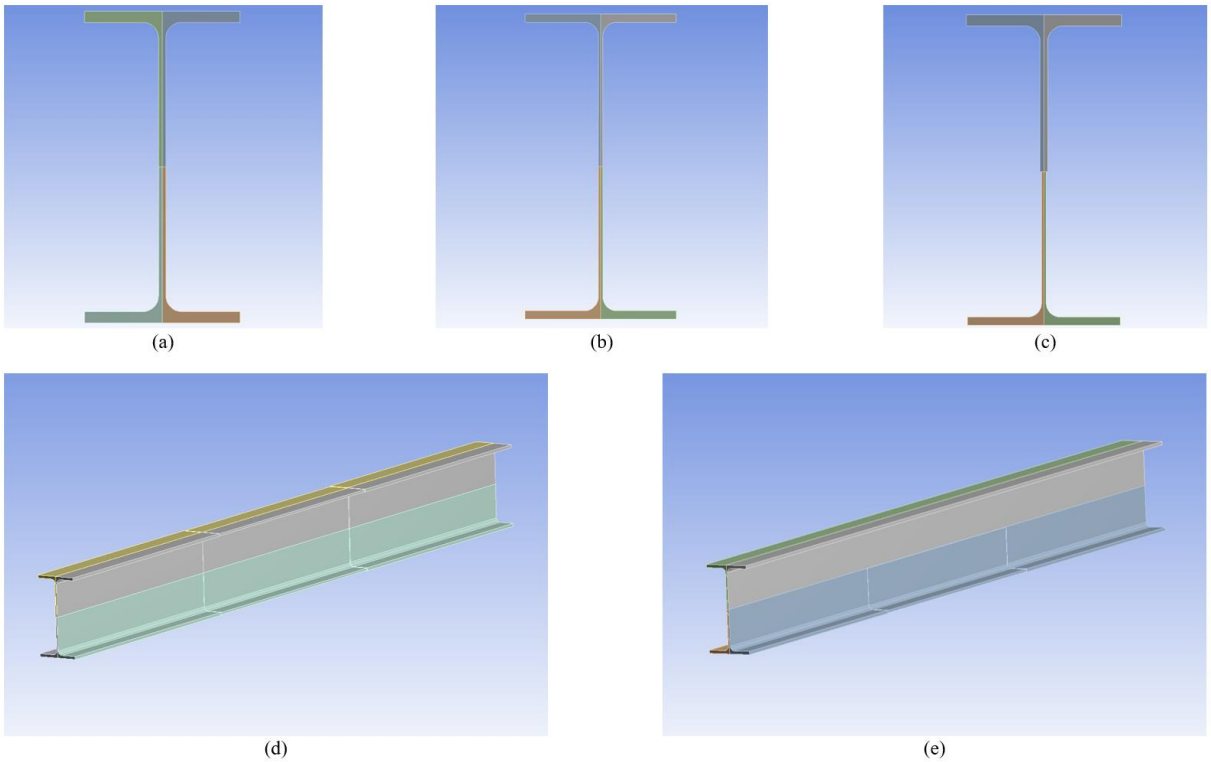

Figure 5-4: Illustration of the analysed beams. (a) Uncorroded, (b) uniform corrosion on the entire section, (c) uniform corrosion on the bottom half of the section, (d) Uniform corrosion around the entire section on the middle of the beam, and (e) uniform corrosion on the bottom half of the middle of the beam.

A preliminary analysis was carried out to determine the most suitable mesh. The mesh refinement is program controlled for all the faces of the beam. The element size can be manually determined. The mesh is set to 5 mm for all faces in this analysis. A larger mesh will decrease the computational cost, but the results will be less accurate.

The boundary conditions are specified in Figure 5-5 and Table 5-2. This type of boundary condition allows rotation about the x-axis. However, rotation about the z-axis is restricted [19].

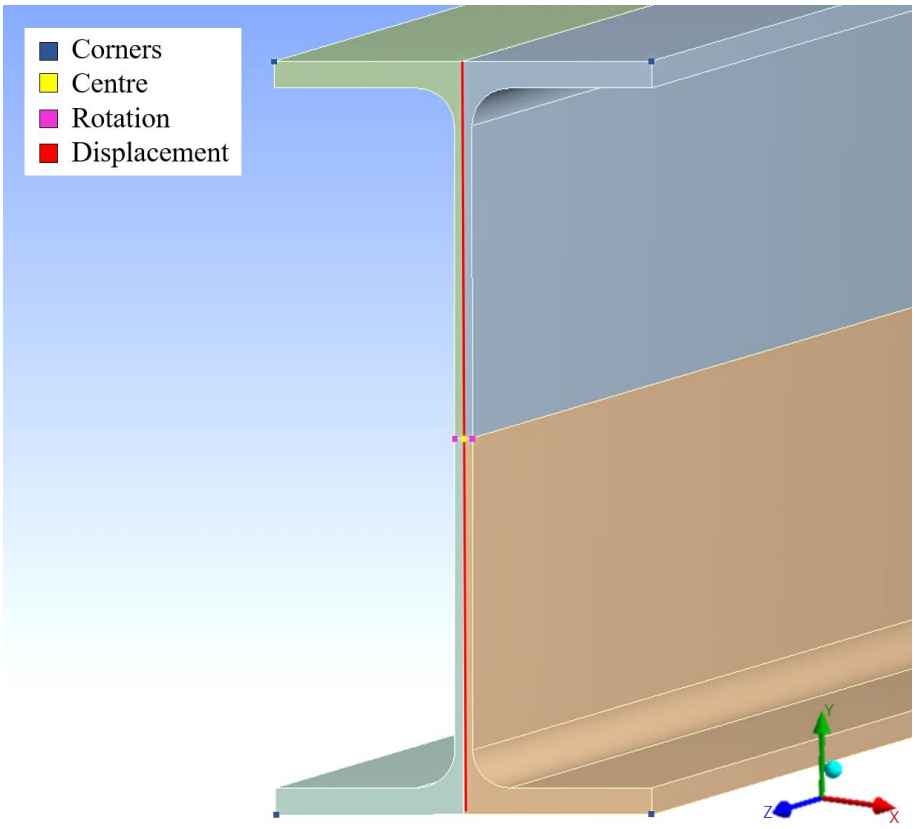

Figure 5-5: Location of the applied boundary conditions

Table 5-2: Boundary conditions

	U_x	U_y	U_z
Corner	0	0	-
Centre	0	-	0
Rotation	-	0	-
Displacement	-	0	-

In this analysis, the top flange is subjected to *line pressure* in the middle of the flange, as shown in Figure 5-6. The applied value for the line pressure in ANSYS Workbench is *w*. This can be calculated from Equation 5.2-1. The eigenvalue obtained from the eigenvalue buckling is multiplied by the applied bending moment *M* to determine the elastic critical moment.

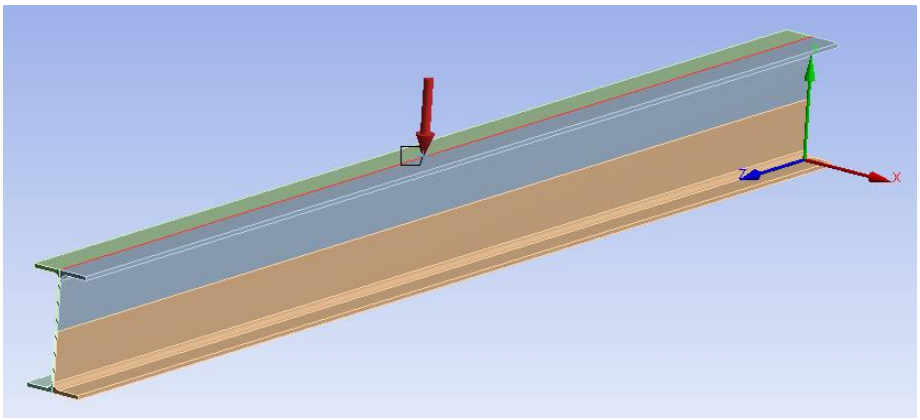

Figure 5-6: The applied line pressure

$$M = \frac{w \cdot L^2}{8} \rightarrow w = \frac{M \cdot 8}{L^2} \qquad \text{Eq. 5.2-1}$$

ANSYS is told to solve the problem for six buckling modes. This will provide six different buckling mode shapes and values. The negative eigenvalues are neglected. For the most conservative design, the lowest positive eigenvalue can be assumed as the solution. This is the first value reached when applying an external load to the beam.

The obtained elastic critical moment from the FE analysis will be combined with the equations from the Eurocode 3 to provide the non-dimensional slenderness ratio, buckling reduction factor, and LTB moment capacity. When calculating the non-dimensional slenderness ratio, buckling reduction factor, and LTB moment capacity for the beams subjected to corrosion case 3 and 4, only the plastic section modulus and the imperfection factor for the corroded middle part of the beam will be employed, as this is the most critical part of the beam when it comes to LTB. Currently, no methods exist to calculate the LTB moment capacity of beams with varying cross-sections.

For the nonlinear buckling analysis, the selected buckling mode shape from the linear Eigenvalue buckling analysis is shared with section C in the flow chart. The scale factor is determined in Equation 5.2-2. L is the beam length of the considered beam in millimetres.

$$c = \frac{L}{1000} \qquad \text{Eq. 5.2-2}$$

5.3 Results

The following figures show the selected modes for the linear eigenvalue buckling for the analysed beams.

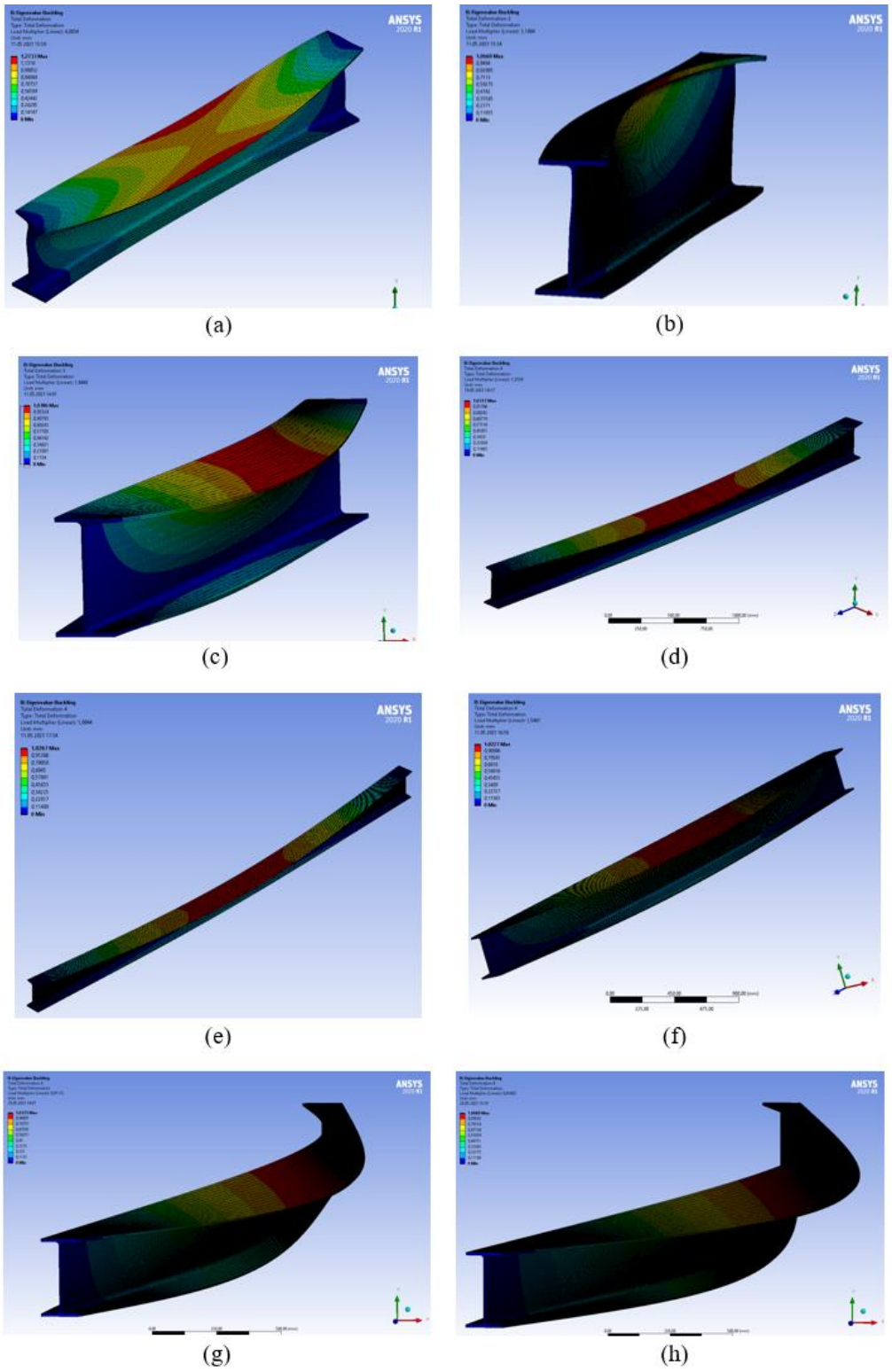

Figure 5-7: The selected buckling mode for the uncorroded section of beam length (a) 1.5m, (b) 2m, (c) 3m, (d) 4m, (e) 5m, (f) 6m, (g) 10m, and (h) 15m

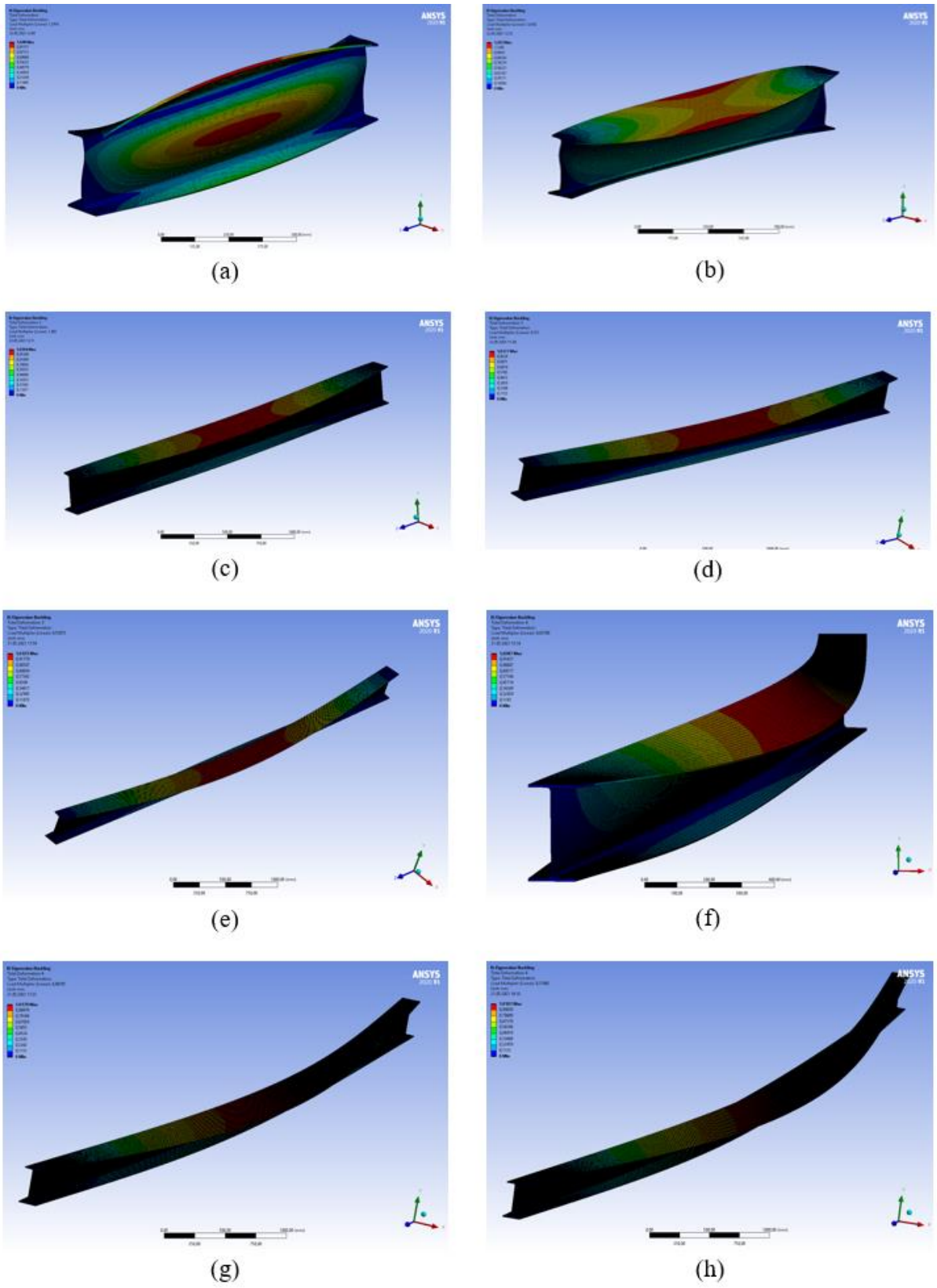

Figure 5-8: The selected buckling mode for the section subjected to corrosion case 1, with beam length (a) 1.5m, (b) 2m, (c) 3m, (d) 4m, (e) 5m, (f) 6m, (g) 10m, and (h) 15m

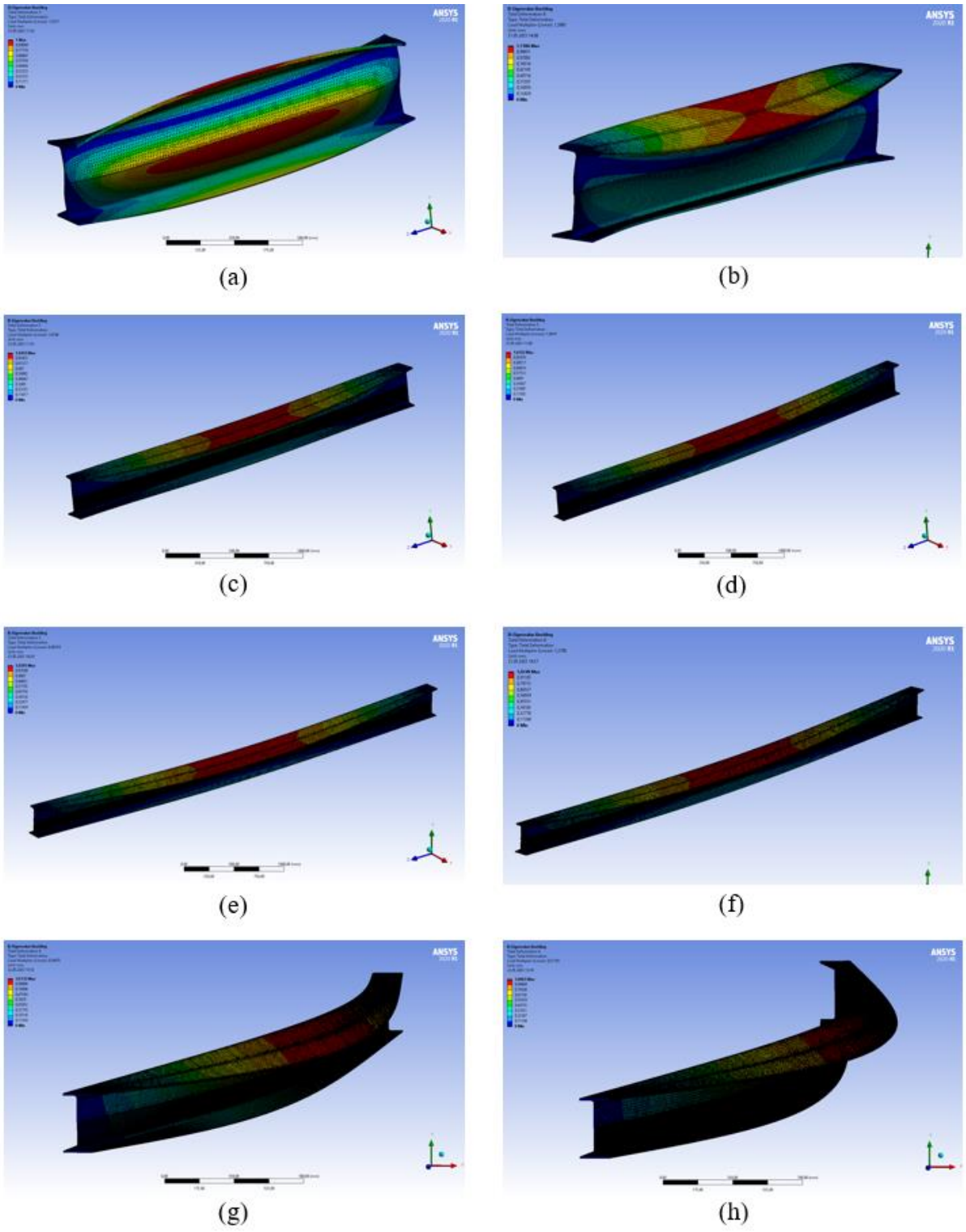

Figure 5-9: The selected buckling mode for the section subjected to corrosion case 2, with beam length (a) 1.5m, (b) 2m, (c) 3m, (d) 4m, (e) 5m, (f) 6m, (g) 10m, and (h) 15m

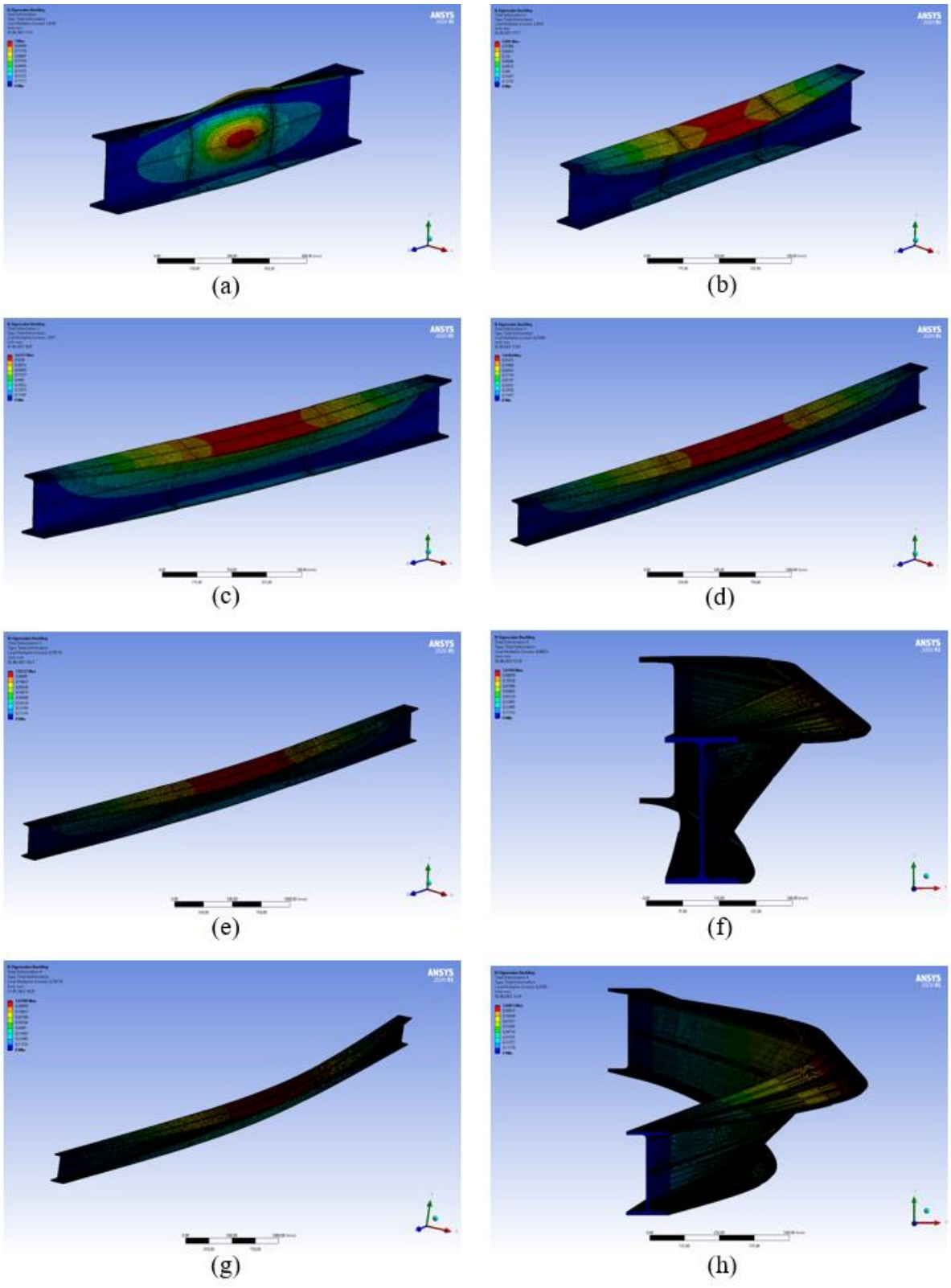

Figure 5-10: The selected buckling mode for the section subjected to corrosion case 3, with beam length (a) 1.5m, (b) 2m, (c) 3m, (d) 4m, (e) 5m, (f) 6m, (g) 10m, and (h) 15m

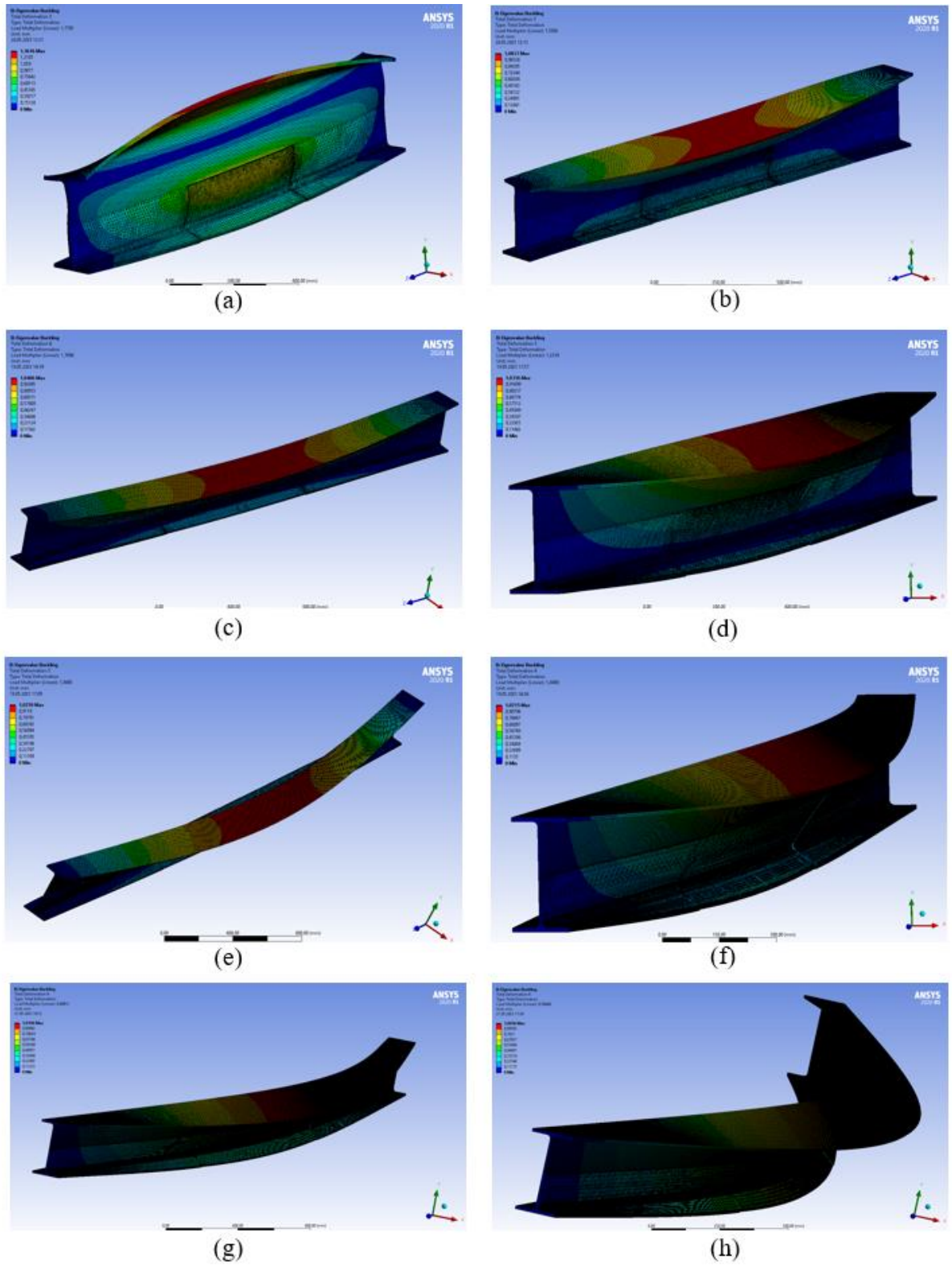

Figure 5-11: The selected buckling mode for the section subjected to corrosion case 4, with beam length (a) 1.5m, (b) 2m, (c) 3m, (d) 4m, (e) 5m, (f) 6m, (g) 10m, and (h) 15m

The following tables contain the elastic critical moment (M_{cr}) obtained from the linear FE analysis in ANSYS Workbench, and the calculated non-dimensional slenderness ratio ($\bar{\lambda}_{LT}$), buckling reduction factor (χ_{LT}), and LTB moment capacity ($M_{b,Rd}$).

Table 5-3: Elastic critical moment, non-dimensional slenderness ratio, buckling reduction factor, and lateral torsional buckling moment capacity for the uncorroded section.

L (m)	$\boldsymbol{M_{cr}}$ **(kNm)**	$\bar{\boldsymbol{\lambda}}_{\boldsymbol{LT}}$	$\boldsymbol{\chi_{LT}}$	$\boldsymbol{M_{b,Rd}}$ **(kNm)**
	FEA	**EC3**	**EC3**	**EC3**
1.5	400.3	0.64	0.87	144.5
2	318.8	0.72	0.84	138.7
3	184.6	0.95	0.70	116.2
4	125.3	1.15	0.56	93.1
5	95.2	1.32	0.46	76.1
6	77.3	1.46	0.39	64.3
10	45.6	1.91	0.24	40.3
15	30.8	2.32	0.17	28.0

Table 5-4: Elastic critical moment, non-dimensional slenderness ratio, buckling reduction factor, and lateral torsional buckling moment capacity for the cross-section subjected to corrosion case 1.

L (m)	$\boldsymbol{M_{cr}}$ **(kNm)**	$\bar{\boldsymbol{\lambda}}_{\boldsymbol{LT}}$	$\boldsymbol{\chi_{LT}}$	$\boldsymbol{M_{b,Rd}}$ **(kNm)**
	FEA	**EC3**	**EC3**	**EC3**
1.5	139.2	0.91	0.65	75.6
2	161.4	0.85	0.70	80.4
3	108.3	1.03	0.58	66.6
4	72.1	1.26	0.44	51.3
5	53.0	1.48	0.35	40.6
6	41.9	1.66	0.29	33.4
10	23.4	2.22	0.17	20.0
15	15.5	2.73	0.12	13.7

Table 5-5: Elastic critical moment, non-dimensional slenderness ratio, buckling reduction factor, and lateral torsional buckling moment capacity for the cross-section subjected to corrosion case 2.

L (m)	M_{cr} (kNm)	$\bar{\lambda}_{LT}$	χ_{LT}	$M_{b,Rd}$ (kNm)
	FEA	**EC3**	**EC3**	**EC3**
1.5	270.7	0.70	0.78	104.5
2	261.3	0.72	0.78	103.6
3	161.5	0.91	0.65	87.5
4	108.2	1.11	0.53	70.6
5	80.1	1.29	0.43	57.6
6	63.5	1.45	0.36	48.2
10	34.9	1.96	0.22	29.1
15	21.8	2.48	0.14	19.0

Table 5-6: Elastic critical moment, non-dimensional slenderness ratio, buckling reduction factor, and lateral torsional buckling moment capacity for the cross-section subjected to corrosion case 3.

L (m)	M_{cr} (kNm)	$\bar{\lambda}_{LT}$	χ_{LT}	$M_{b,Rd}$ (kNm)
	FEA	**EC3**	**EC3**	**EC3**
1.5	261.7	0.66	0.80	92.8
2	254.8	0.67	0.80	92.2
3	149.7	0.88	0.68	78.0
4	103.4	1.06	0.56	64.8
5	79.2	1.21	0.47	54.7
6	64.8	1.34	0.41	47.4
10	38.4	1.73	0.27	31.0
15	26.0	2.11	0.19	22.0

Table 5-7: Elastic critical moment, non-dimensional slenderness ratio, buckling reduction factor, and lateral torsional buckling moment capacity for the cross-section subjected to corrosion case 4.

L (m)	M_{cr} (kNm)	$\bar{\lambda}_{LT}$	χ_{LT}	$M_{b,Rd}$ (kNm)
	FEA	EC3	EC3	EC3
1.5	354.1	0.61	0.83	110.9
2	301.8	0.67	0.80	107.3
3	179.0	0.86	0.68	91.4
4	122.3	1.05	0.57	76.0
5	92.3	1.20	0.48	63.7
6	74.4	1.34	0.41	54.5
10	42.3	1.78	0.26	34.4
15	27.3	2.21	0.17	23.3

The result from the nonlinear buckling analysis of the 3 m long beam subjected to corrosion case 1 is plotted in Figure 5-12. As a result, the LTB moment capacity of this beam is 76.4 kNm.

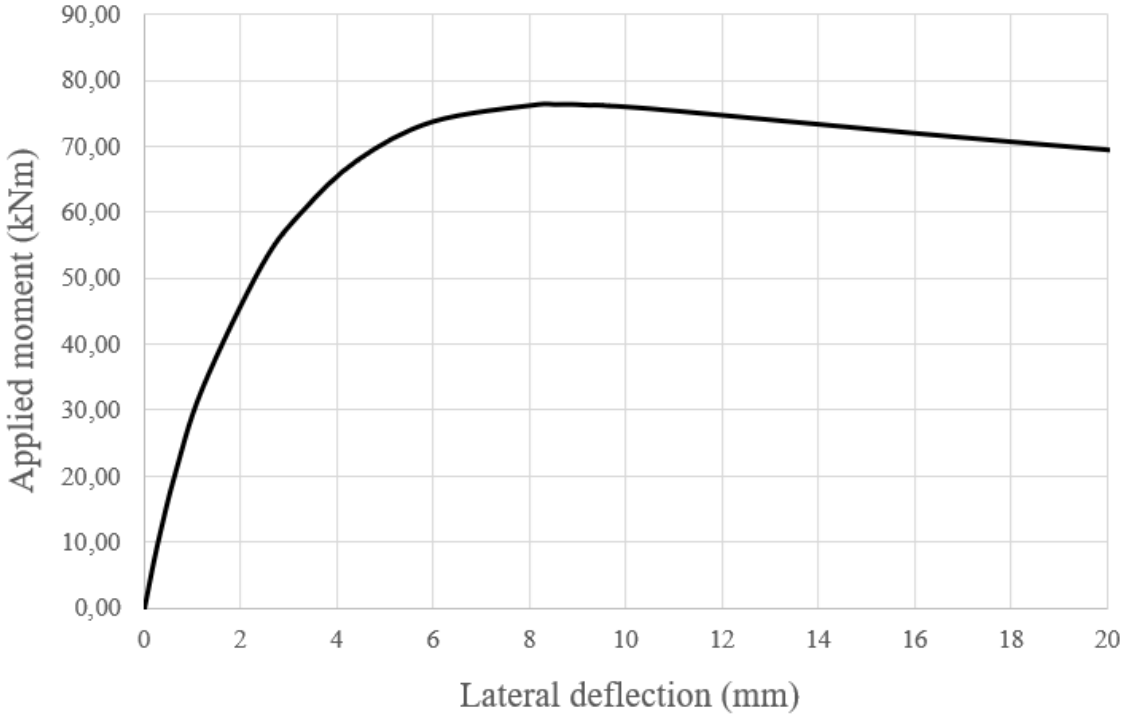

Figure 5-12: Applied moment versus lateral deflection for the 3 m long beam subjected to corrosion case 1

6 Comparison of results and discussion

This study is based on conservative values for the corrosion depth and pattern on the cross-sections. Only uniform corrosion is applied to the beams in this study, while crevice and pitting corrosion are neglected. For a steel beam subjected to corrosion, the corrosion depth will not be constant for the entire beam length or section. Only a linear analysis is performed for most of the beams for the FE approach to obtain the elastic buckling moment, which is used to calculate the LTB moment capacity based on the guidelines given in Eurocode 3. This may be less accurate than the nonlinear FE analysis-based LTB capacities.

Table 6-1 provides the obtained elastic critical moment for all the corrosion scenarios and beam lengths included in this study. The LTB moment capacities for the same beams are provided in Table 6-2. These tables compare the analytical results with the results from the linear FE analysis. There is a significant difference in the LTB moment capacity for the shortest beams. For the longer beams, the difference decreases. The LTB moment capacity obtained from the FE analysis is more conservative than the analytical LTB moment capacity. The result from the nonlinear buckling analysis of the 3 m long beam subjected to corrosion case 1 provides an LTB moment capacity of 76.4 kNm. This is less than the analytical LTB moment capacity, yet greater than the LTB moment capacity based on the elastic critical moment obtained by the linear FE analysis.

The 15 m long beam subjected to corrosion case 1 has the lowest LTB moment capacity. In this case, the capacity is reduced by 51% compared to the uncorroded beam. This is expected, as sections subjected to corrosion case 1 are most affected by thickness loss. For the 15 m long beam subjected to corrosion case 3, the LTB moment capacity is reduced by 21%. This indicates that the length of the corroded part of the beam influences the LTB moment capacity. The longer the corroded section is, the lower the LTB moment capacity.

The LTB moment capacity is expected to increase when the beam length is decreased. Thus, the results from the linear FE analysis show that the 1.5 m long beam subjected to corrosion case 1 has a lower LTB moment capacity than the 2 m long beam subjected to the corrosion scenario. A combination of local buckling and LTB may be the reason, as short beams are more likely to be subjected to local plate buckling.

Table 6-1: The elastic critical moment provided by the analytical ($M_{cr,A}$) and the FE approach ($M_{cr,B}$)

L (m)	No corrosion		Case 1		Case 2		Case 3		Case 4	
	$M_{cr,A}$	$M_{cr,B}$	$M_{cr,A}$	$M_{cr,B}$	$M_{cr,A}$	$M_{cr,B}$	$M_{cr,A}$	$M_{cr,B}$	$M_{cr,A}$	$M_{cr,B}$
1.5	955.1	400.3	647.1	139.2	788.8	270.7	-	261.7	-	354.1
2	557.5	318.8	371.4	161.4	457.8	261.3	-	254.8	-	301.8
3	271.8	184.6	174.1	108.3	220.5	161.5	-	149.7	-	179.0
4	170.0	125.3	104.7	72.1	136.3	108.2	-	103.4	-	122.3
5	121.5	95.2	72.1	53.0	96.4	80.1	-	79.2	-	92.3
6	94.0	77.3	54.1	41.9	74.0	63.5	-	64.8	-	74.4
10	49.4	45.6	26.4	23.4	38.2	34.9	-	38.4	-	42.3
15	31.3	30.8	16.1	15.5	24.0	21.8	-	26.0	-	27.3

Table 6-2: The LTB moment capacity provided from the analytical ($M_{bRd,A}$) and the FE approach ($M_{bRd,B}$)

L (m)	No corrosion		Case 1		Case 2		Case 3		Case 4	
	$M_{bRd,A}$	$M_{bRd,B}$	$M_{bRd,A}$	$M_{bRd,B}$	$M_{bRd,A}$	$M_{bRd,B}$	$M_{bRd,A}$	$M_{bRd,B}$	$M_{bRd,A}$	$M_{bRd,B}$
1.5	157.0	144.5	105.9	75.6	123.2	104.5	-	92.8	-	110.9
2	150.6	138.7	99.0	80.4	115.8	103.7	-	92.2	-	107.3
3	133.6	116.2	82.6	66.6	98.6	87.5	-	78.0	-	91.4
4	111.7	93.1	65.3	51.3	80.6	70.7	-	64.8	-	76.0
5	91.2	76.1	51.3	40.6	65.6	57.6	-	54.7	-	63.7
6	75.4	64.3	41.2	33.4	54.3	48.2	-	47.4	-	54.5
10	43.4	40.3	22.3	20.0	31.5	29.1	-	31.0	-	34.4
15	28.5	28.0	14.2	13.7	20.8	19.0	-	22.0	-	23.3

In the following plots, the results from the analytical and the FE approach of the uncorroded section and the sections subjected to corrosion case 1 and 2 are plotted. The plots are buckling reduction factor (χ_{LT}) versus non-dimensional slenderness ratio ($\bar{\lambda}_{LT}$), LTB moment capacity (M_{bRd}) versus non-dimensional slenderness ratio, and LTB moment capacity versus beam length.

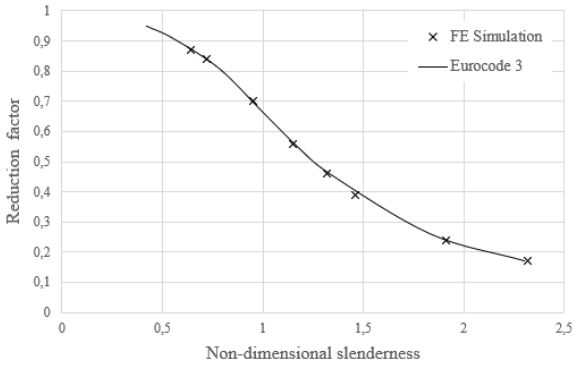

Figure 6-1: Buckling reduction factor versus non-dimensional slenderness for the uncorroded section

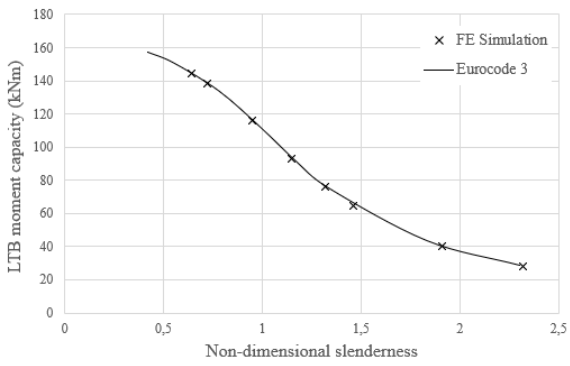

Figure 6-2: LTB moment capacity versus non-dimensional slenderness ratio for the uncorroded section

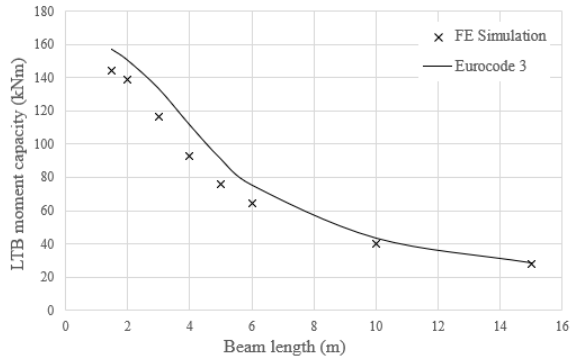

Figure 6-3: LTB moment capacity versus beam length for the uncorroded section

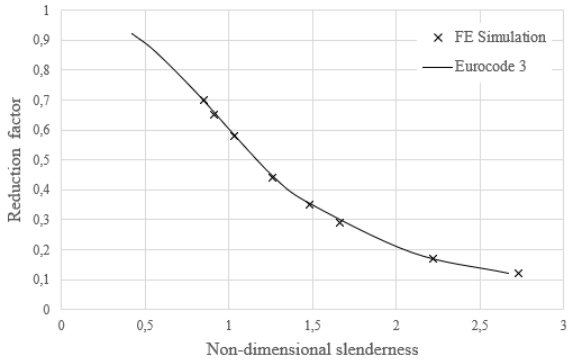

Figure 6-4: Buckling reduction factor versus non-dimensional slenderness for the section subjected to corrosion case 1

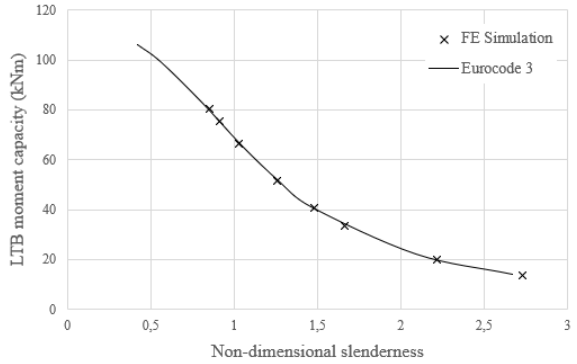

Figure 6-5: LTB moment capacity versus non-dimensional slenderness ratio for the section subjected to corrosion case 1

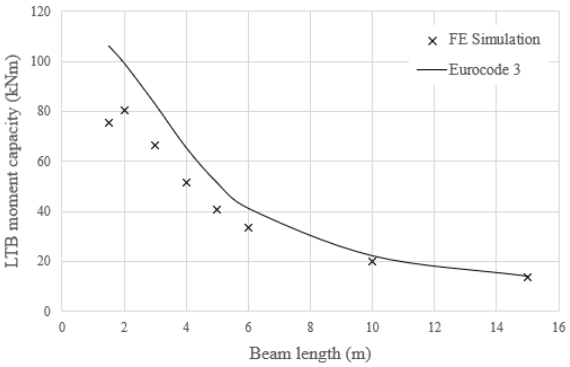

Figure 6-6: LTB moment capacity versus beam length for the section subjected to corrosion case 1

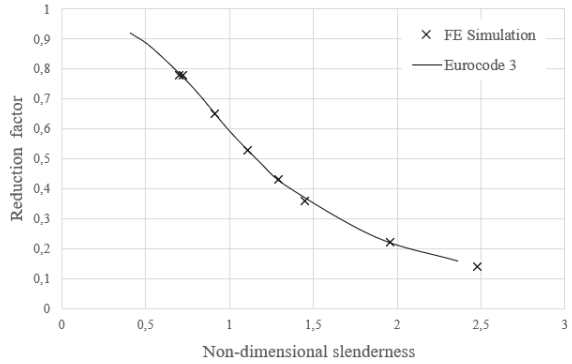

Figure 6-7: Buckling reduction factor versus non-dimensional slenderness for the section subjected to corrosion case 2

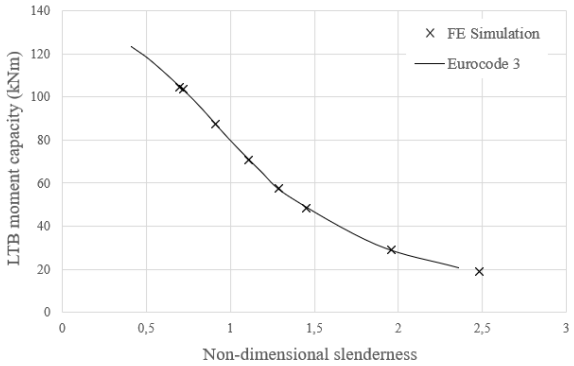

Figure 6-8: LTB moment capacity versus non-dimensional slenderness ratio for the section subjected to corrosion case 2

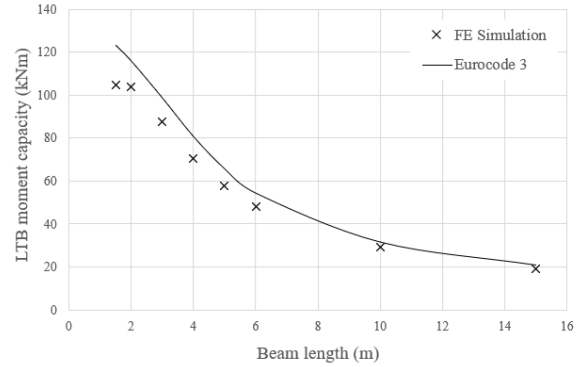

Figure 6-9: LTB moment capacity versus beam length for the section subjected to corrosion case 2

In the following plots, the buckling reduction factor versus non-dimensional slenderness ratio are plotted for the corrosion case 3 and 4.

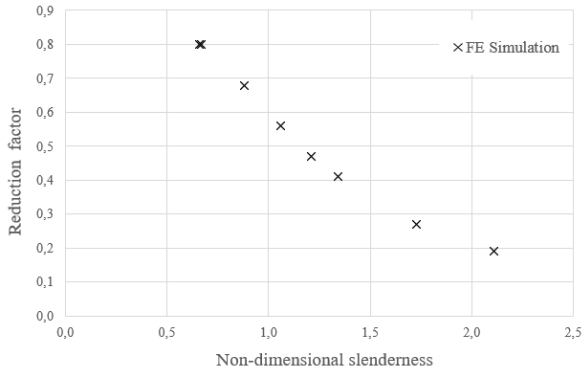

Figure 6-10: Buckling reduction factor versus non-dimensional slenderness for the section subjected to corrosion case 3

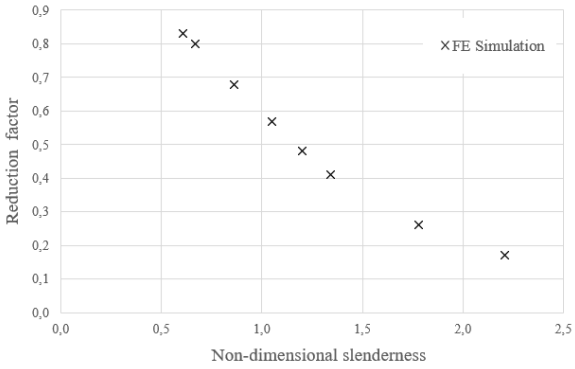

Figure 6-11: Buckling reduction factor versus non-dimensional slenderness for the section subjected to corrosion case 4

7 Conclusions

7.1 Summary

In this thesis, the remaining LTB moment capacities of IPE300-sections subjected to four different corrosion scenarios are studied. The corrosion scenario and beam length are used as parameters. The utilised approaches are based on Eurocode 3 and the elastic critical moment obtained by the linear FE analysis in ANSYS Workbench. A nonlinear FE buckling simulation is provided for one beam. The objective is to study how various scenarios of uniform corrosion affect the remaining LTB moment capacity for IPE300-sections, and to provide an analytical framework for I-beams with varying cross-sections.

Theory for determining the remaining LTB moment capacity for corroded beams, where the cross-section is constant for the entire beam, is provided. In the analytical approach, this theory is used to calculate the elastic critical moment (M_{cr}), non-dimensional slenderness ratio ($\bar{\lambda}_{LT}$), buckling reduction factor (χ_{LT}), and LTB moment capacity ($M_{b,Rd}$) for the uncorroded section, and the cross-sections subjected to corrosion case 1 and 2.

ANSYS Workbench is utilised for the linear FE simulation. The elastic critical moment (M_{cr}) is provided from the simulation. This is then employed to calculate the non-dimensional slenderness ratio ($\bar{\lambda}_{LT}$), reduction factor (χ_{LT}), and LTB moment capacity ($M_{b,Rd}$) for the uncorroded section, and the sections subjected to corrosion case 1, 2, 3, and 4. The results for the uncorroded section and sections subjected to corrosion case 1 and 2 are compared with the results from the analytical approach.

7.2 Concluding remarks

Based on the comparison of the results from the analytical approach and the linear FE approach, the linear LTB moment capacity is more conservative than the analytical LTB moment capacity. The result from the nonlinear buckling analysis is less conservative than the linear analysis, yet more conservative than the analytical approach. However, it is necessary to have more data to make a certain conclusion regarding the nonlinear buckling capacity.

The 15 m long beam subjected to corrosion case 1 has the lowest LTB moment capacity, as this section is most affected by thickness loss. In this case, the capacity is reduced by 51% compared to the uncorroded beam. For the 15 m long beam subjected to corrosion case 3, the

LTB moment capacity is reduced by 21%. This proves that the length of the corroded section affects the LTB moment capacity of the beams.

For some of the shortest beams, the linear LTB moment capacity deviates from the analytical LTB moment capacity due to local plate buckling.

7.3 Further work

Upcycling of steel is a complicated process that will depend on more factors than just the remaining capacity of the structural elements. For further studies, it will be interesting to study how fatigue, decommissioning, and rust removal affect the remaining capacity. Hence, it is essential to establish an upcycling process that is more economical for the industry than recycling steel. New structures should be designed to be straightforward to reuse to ensure the future reuse of structural elements.

For further work, performing an experimental study of corroded beams comparing the experimental and analytical results would be interesting. Due to time limitations and high computational costs, a nonlinear buckling analysis is only performed for one beam. It would be interesting to perform a nonlinear buckling analysis on the rest of the beams. Further recommendations are to repeat the parametric study to include various cross-sections and corrosion patterns.

References

[1] H. F. Gholipour, A. Arjomandi and S. Yam, «Green property finance and CO2 emissions in the building industry,» *Elsevier,* vol. 51, Feb. 2022, art no. 100696. doi: https://doi.org/10.1016/j.gfj.2021.100696

[2] The Ministry of Petroleum and Energy and the Norwegian Petroleum Directorate, «Cessation and decommissioning.» Norskpetroleum.no. Available: https://www.norskpetroleum.no/en/developments-and-operations/cessation-and-decommissioning/ (Accessed: 24.02.23).

[3] G. P. da Ponte Jr. *Risk Management in the Oil and Gas Industry,* 1. Ed. Oxford, England: Gulf Professional Publishing, 2021.

[4] J. Meling, R. E. Hausmann and E. Faulds, «Avslutning og disponering av utrangerte innretninger,». Dr.techn.Olav Olsen AS, Norway, 12635-01-OO-R-001, April 4, 2018. [Online]. Available: https://www.npd.no/globalassets/1-npd/publikasjoner/rapporter/markedsrapport.pdf

[5] Nordic Circles. «How do we upcycle steel?» Nordiccircles.com. Available: https://www.nordiccircles.com/upcycling (Accessed: 02.03.23).

[6] R. Rahgozar, «Remaining capacity assessment of corrosion damaged beams using minimum curves,» *Elsevier*, vol. 65, no. 2, p. 299-307, Feb. 2008. doi: https://doi.org/10.1016/j.jcsr.2008.02.004

[7] *Eurocode 3: Design of steel structures part 1-1: General rules and rules for buildings*, NS-EN 1993-1:2005+A1:2014+NA:2015, 2015.

[8] Y. Sharifi & R. Rahgozar, « Evaluation of the remaining lateral torsional buckling capacity in corroded steel members,» *Journal of Zhejiang University*, vol. 11, p. 887-897, 2010. doi: https://doi.org/10.1631/jzus.A0900673

[9] K. Trethewey and J. Chamberlain. *Corrosion: For science and engineering*, 2. Ed. Published in Harlow, England: Pearson Education, 1995.

[10] A. Aeran, S. C. Siriwardane, O. Mikkelsen and I. Langen, «A framework to assess structural integrity of ageing offshore jacket structures for life extension,» *Elsevier*, vol. 56, p. 237-259, Nov. 2017. doi: https://doi.org/10.1016/j.marstruc.2017.08.002

[11] S. N. Karlsdottir. «Corrosion, Scaling and Material Selection in Geothermal Power Production,» in *Comprehensive Renewable Energy*. Sayigh, 1. Ed, Oxford, England: Elsevier, 2012, p. 239-256.

[12] M. Otutu. «Impressed Current Cathodic Protection.» Corrosionpedia.com. Available: https://www.corrosionpedia.com/definition/1237/impressed-current-cathodic-protection-iccp (Accessed: 05.04.23).

[13] G. Koch, G. Ripley & D. McKay, «The New Risk Perspective in Corrosion Management,» *ASME*, Jul. 2018. doi: https://doi.org/10.1115/MTS2013-0313

[14] N. D. Adasooriya and S. C. Siriwardane, «Remaining fatigue life estimation of corroded bridge members,» *FFEMS*, vol.37, no. 6, 603-622, Jan. 2014. doi: https://doi.org/10.1111/ffe.12144

[15] G. Kullashi, S. C. Siriwardane and M. A. Atteya, «Lateral torsional buckling capacity of corroded steel beams: A parametric study,» *IOP Publishing*, 2021. doi: 10.1088/1757-899X/1201/1/012038

[16] The Ministry of Petroleum and Energy and the Norwegian Petroleum Directorate. «Gyda.» Norskpetroleum.no. Available: https://www.norskpetroleum.no/fakta/felt/gyda/ (Accessed: 12.04.23).

[17] N. S. Trahair, M. A. Bradford, D. A. Nethercot and L. Gardner. *The behaviour and design of steel structures to EC3*, 4. Ed. London, England: Taylor & Francis, 2008.

[18] ANSYS. «Buckling.» Ansys.com. Available at: https://courses.ansys.com/wp-content/uploads/2021/01/Lesson3-Buckling.pdf (Accessed: 03.05.23).

[19] A. Rossi, D. H. Saito, C. H. Martins and A. S. C. de Souza, «The influence of structural imperfections on the LTB strength of I-beams,» *Structures*, vol. 29, p. 1173-1186, Feb. 2021. doi: https://doi.org/10.1016/j.istruc.2020.11.020

Appendix

A: Uncorroded section

Appendix A consists of the MATLAB code utilised in Chapter 4 for the uncorroded section. The beam length L is changed according to what beam length is calculated.

```
% Lateral torsional buckling moment capacity of IPE300
% No corrosion
clear           % Clear all variables
clc             % Clear command window

% Dimensions (mm)
h=300;          % Section height
b=150;          % Section width
tw=7.1;         % Web thickness
tf=10.7;        % Flange thickness
L=6000;         % Beam length
Cw=h-2*tf;      % Web height

E=210*10^3;     % N/mm^2
G=81395;        % N/mm^2
fy=275;         % MPa
epsilon=sqrt(235/fy);
alfaM=1.13;     % Moment modification factor
gammaM=1;       % Safety factor (Neglected)

% Class classification
if (h-2*tf)/(tw*epsilon) <= 72 % Web
    "Web: Class 1"
else
    "Web: Not class 1"
end

if ((b-tw)/2)/(tf*epsilon) <= 9 % Flange
    "Flange: Class 1"
else
    "Flange: Not class 1"
end

% Moment of inertia about z-z axis (mm^4)
Iz= 2*(1/12*tf*b^3)+(1/12*(Cw*tw^3))

% Torsion constant (mm^4)
It=2*(1/3*b*tf^3)+1/3*Cw*tw^3

% Warping constant (mm^6)
Iw=(b^3*(h-tf)^2*tf)/24

% Critical elastic moment (Nmm)
Mcr=(sqrt(((pi^2*E*Iz)/L^2)*((G*It)+((pi^2*E*Iw)/L^2))))*alfaM

% Plastic section modulus (mm^3)
Wply=(b*tf*(h-tf)/2)*2+((h/2-tf)*tw*(h/2-tf)/2)*2

% Imperfection factor
if h/b <= 2
    alfaLT=0.21;
else
    alfaLT=0.34;
end
```

```
% Slenderness ratio for buckling
lambdaLT=sqrt((fy*Wply)/Mcr)

% Function used to define the reduction factor
phiLT=0.5*(1+alfaLT*(lambdaLT-0.2)+(lambdaLT)^2);

% Reduction factor for buckling
chiLT=1/(phiLT+sqrt(phiLT^2-lambdaLT^2));

% Lateral torsional buckling moment capacity (kNm)
Mbrd=(chiLT*Wply*fy/gammaM)*10^(-6)
```

B: Corrosion case 1

Appendix B presents the MATLAB code utilised in Chapter 4 for the section subjected to uniform corrosion over the entire cross-section. The beam length *L* is changed according to what beam length is calculated.

```
% Lateral torsional buckling moment capacity of IPE300
% Uniform corrosion all over the section
clear           % Clear all variables
clc             % Clear command window

% Corrosion wastage
A=0.1;          % Parameter for offshore structures
B=0.823;        % Parameter for offshore structures
t=30;           % Lifespan of structure (years)
t0=5;           % Lifespan of corrosion protection (years)
w=A*(t-t0)^B;   % Corrosion wastage (mm)

% Dimensions (mm)
h=300-2*w;      % Section height
b=150-2*w;      % Section width
tw=7.1-2*w;     % Web thickness
tf=10.7-2*w;    % Flange thickness
L=3000;         % Beam length
Cw=h-2*tf;      % Web height

E=210*10^3;     % N/mm^2
G=81395;        % N/mm^2
fy=275;         % MPa
epsilon=sqrt(235/fy);
gammaM=1;       % Safety factor (Neglected)
alfaM=1.13;     % Moment modification factor

% Class classification
if (h-2*tf)/(tw*epsilon) <= 72 % Web
    "Web: Class 1"
else
    "Web: Not class 1"
end

if ((b-tw)/2)/(tf*epsilon) <= 9 % Flange
    "Flange: Class 1"
elseif ((b-tw)/2)/(tf*epsilon) <= 10
    "Flange: Class 2"
else
    "Flange: Class 3 or 4"
end

% Moment of inertia about z-z axis (mm^4)
Iz= 2*(1/12*tf*b^3)+(1/12*(Cw*tw^3))

% Torsion constant (mm^4)
It=2*(1/3*b*tf^3)+1/3*Cw*tw^3

% Warping constant (mm^6)
Iw=(b^3*(h-tf)^2*tf)/24

% Critical elastic moment (Nmm)
Mcr=(sqrt(((pi^2*E*Iz)/L^2)*((G*It)+((pi^2*E*Iw)/L^2))))*alfaM
```

```
% Plastic section modulus (mm^3)
Wply=(b*tf*(h-tf)/2)*2+((h/2-tf)*tw*(h/2-tf)/2)*2

% Imperfection factor
if h/b <= 2
    alfaLT=0.21;
else
    alfaLT=0.34;
end

% Slenderness ratio for buckling
lambdaLT=sqrt((fy*Wply)/Mcr)

% Function used to define the reduction factor
phiLT=0.5*(1+alfaLT*(lambdaLT-0.2)+(lambdaLT)^2);

% Reduction factor for buckling
chiLT=1/(phiLT+sqrt(phiLT^2-lambdaLT^2));

% Lateral torsional buckling moment capacity (kNm)
Mbrd=(chiLT*Wply*fy/gammaM)*10^(-6)
```

C: Corrosion case 2

Appendix C consists of the MATLAB code employed in Chapter 4 for the section subjected to uniform corrosion on the bottom flange and bottom half of the web. The beam length L is changed according to what beam length is calculated.

```
% Lateral torsional buckling moment capacity of IPE300
% Uniform corrosion on bottom flange and bottom half of web
clear           % Clear all variables
clc             % Clear command window

% Corrosion wastage
A=0.1;          % Parameter for offshore structures
B=0.823;        % Parameter for offshore structures
t=30;           % Lifespan of structure (years)
t0=5;           % Lifespan of corrosion protection (years)
w=A*((t-t0)^B); % Corrosion wastage (mm)

% Dimensions (mm)
h=300-w;        % Section height
b=150;          % Section width: Top (No corrosion)
bc=150-2*w;     % Section width: Bottom (Corrosion)
tw=7.1;         % Web thickness: Top half (No corrosion)
twc=7.1-2*w;    % Web thickness: Bottom half (Corrosion)
tf=10.7;        % Flange thickness: Top flange (No corrosion)
tfc=10.7-2*w;   % Flange thickness: Bottom flange (Corrosion)
L=15000;        % Beam length
Cw=300-tf-tfc;  % Web height

E=210*10^3;     % N/mm^2
G=81395;        % N/mm^2
fy=275;         % MPa
epsilon=sqrt(235/fy);
gammaM=1;       % Safety factor (Neglected)
alfaM=1.13;     % Moment modification factor

% Plastic neutral axis (mm)
yp=((h*tw)-(tfc*tw)-((Cw/2)*tw)+((Cw/2)*twc)+(bc*tfc)-(b*tf)+(tf*tw))/(2*tw);

% Tension part
At1=b*tf;
At2=(yp-tf)*tw;
yt1=yp-tf/2;
yt2=(yp-tf)/2;

% Compression part
Ac1=bc*tfc;
Ac2=(Cw/2)*twc;
Ac3=(h-yp-tfc-Cw/2)*tw;
yc1=h-yp-tfc/2;
yc2=h-yp-tfc-Cw/4;
yc3=(h-yp-tfc-Cw/2)/2;

% Plastic section modulus (mm^3)
Wply=At1*yt1+At2*yt2+Ac1*yc1+Ac2*yc2+Ac3*yc3

% Moment of inertia about z-z axis (mm^4)
Iz=5.11*10^6;   % Found in Ansys DesignModeler

% Torsion constant (mm^4)
It=1.06*10^5;   % From Ansys DesignModeler
```

```
% Warping constant (mm^6)
Iw=1.03*10^11;  % Found in Ansys DesignModeler

% Critical elastic moment (Nmm)
Mcr=(sqrt(((pi^2*E*Iz)/L^2)*((G*It)+((pi^2*E*Iw)/L^2))))*alfaM
Mcr/10^6

% Imperfection factor
% If h/b <= 2: alfaLT=0.21
% If h/b > 2: alfaLT=0.34

% h/b=1.9906
% h/bc=2.0288
% Most conservative: h/bc=2.0288 > 2
alfaLT=0.34;

% Slenderness ratio for buckling
lambdaLT=sqrt((fy*Wply)/Mcr)

% Function used to define the reduction factor
phiLT=0.5*(1+alfaLT*(lambdaLT-0.2)+(lambdaLT)^2);

% Reduction factor for buckling
chiLT=1/(phiLT+sqrt(phiLT^2-lambdaLT^2))

% Lateral torsional buckling moment capacity (kNm)
Mbrd=(chiLT*Wply*fy/gammaM)*10^(-6)
```

D: Cross-sectional properties for corrosion case 2

Appendix D represents the cross-sectional properties of the cross-sections subjected to uniform corrosion on the bottom half of the section.

Details View	
Details of Bottomhalf	
Sketch	Bottomhalf
Show Constraints?	No
Dimensions: 7	
H1	150 mm
H2	7,1 mm
H3	4,3 mm
H4	147,2 mm
V5	298,6 mm
V6	10,7 mm
V7	7,9 mm
Edges: 16	
Physical Properties: 10	
A	4363,9 mm²
Ixx	6,6457e+07 mm^4
Ixy	4,1293e-09 mm^4
Iyy	5,1142e+06 mm^4
Iw	1,0342e+11 mm^6
J	1,0577e+05 mm^4
CGx	0 mm
CGy	169,29 mm
SHx	-0,0033491 mm
SHy	174,31 mm

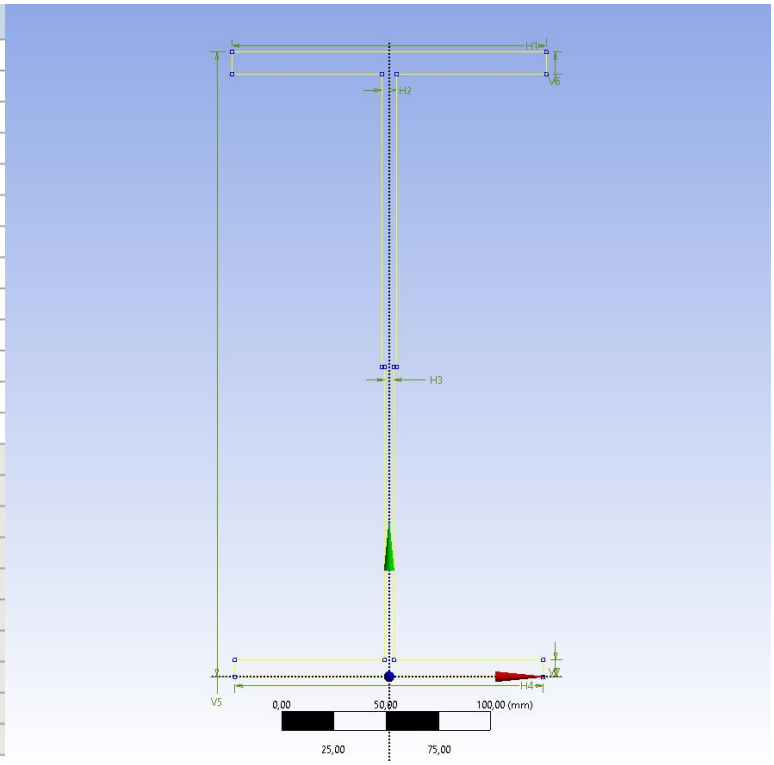

E: $M_{b,Rd}$ with M_{cr} obtained in ANSYS

Appendix E consists of the MATLAB code that utilises the elastic critical moment found in the FE analysis in Chapter 5 to obtain the LTB moment capacity. The elastic critical moment *Mcr* is changed according to the results from the FE analysis. The plastic section modulus *Wply* and imperfection factor *alfaLT* are also changed according to the analysed cross-section.

```
% Lateral torsional buckling moment capacity of IPE300
% Mcr is found in Ansys Workbench
clear                % Clear all variables
clc                  % Clear command window

fy=275;              % MPa
gammaM=1;            % Safety factor (Neglected)

% Plastic section modulus (mm^3)
%Wply=6.02*10^5;     % No corrosion
Wply=4.20*10^5;      % Corrosion case 1 & 3
%Wply=4.86*10^5;     % Corrosion case 2 & 4

% Critical elastic moment obtained in Ansys Workbench (Nmm)
Mcr=161.4*10^6;
Mcr/10^6

% Imperfection factor
%alfaLT=0.21;        % No corrosion
alfaLT=0.34;         % Corrosion case 1 & 3
%alfaLT=0.34;        % Corrosion case 2 & 4

% Slenderness ratio for buckling
lambdaLT=sqrt((fy*Wply)/Mcr)

% Function used to define the reduction factor
phiLT=0.5*(1+alfaLT*(lambdaLT-0.2)+(lambdaLT)^2);

% Reduction factor for buckling
chiLT=1/(phiLT+sqrt(phiLT^2-lambdaLT^2))

% Lateral torsional buckling moment capacity (kNm)
Mbrd=(chiLT*Wply*fy/gammaM)*10^(-6)
```